Cement and Concrete Research 39 (2009) 206–226

Contents lists available at ScienceDirect

Cement and Concrete Research

journal homepage: http://ees.elsevier.com/CEMCON/default.asp

Durability of self-consolidating concrete to sulfate attack under combined cyclic environments and flexural loading

M.T. Bassuoni [a], M.L. Nehdi [b,*]

[a] School of Planning, Architecture and Civil Engineering, Centre for Built Environment Research, Queen's University of Belfast, Belfast BT9 5AG, UK
[b] Department of Civil and Environmental Engineering, The University of Western Ontario, 1151 Richmond St., London, ON, Canada N6A 5B9

ARTICLE INFO

Article history:
Received 11 November 2007
Accepted 4 December 2008

Keywords:
Performance tests
Self-consolidating concrete
C-sulfate attack
E-composite cements
Air-entrainment
E-hybrid fibre reinforcement

ABSTRACT

Classical sulfate immersion tests for concrete have often given different behaviour from that observed in real field exposure. Such tests do not consider other parameters existing in service that can affect the mechanisms and kinetics of sulfate attack. On the other hand, the current shift towards performance-based standards and specifications for concrete requires the development of performance tests that better correlate to field conditions. Such holistic tests can effectively evaluate the service life of normal and emerging types of concrete. With the growing use of self-consolidating concrete (SCC) in various infrastructure applications, it has become necessary to establish reliable data on its durability. In the present study, the durability of a wide range of SCC mixture designs to sulfate attack is assessed when other concomitant damage mechanisms (cyclic environmental conditions and flexural loading) are considered. Based on the tested mixture design variables (type of binders, air-entrainment, sand-to-total aggregates mass ratio, and hybrid fibre reinforcement), potential performance risks (in terms of physico-mechanical parameters) under such a combined exposure were identified. Those risks were not tangible under a full-immersion test method. Thermal, mineralogical and microscopy analyses revealed the coexistence of complex deterioration processes in SCC under the combined exposure, which is fundamentally different from the occurrence of a single damage mechanism (sulfate attack).

1. Introduction

External sulfate attack on cement-based materials has been a key durability issue and a subject of extensive investigation for many decades [1]. Controversy and confusion on this type of attack and its underlying mechanisms led some authors to revisit the topic several times [1–3].

Dissolved sulfate salts can enter into chemical reactions with cement-based materials causing expansion, cracking and spalling, and/or softening and disintegration. The classical form of sulfate attack involves alkali sulfates such as sodium sulfate (Na_2SO_4) which reacts with portlandite (CH), monosulfate and unreacted C_3A to form gypsum ($C\overline{S}H$) and ettringite ($C_6A\overline{S}_3H_{32}$), which can cause expansion, cracking, and deterioration of concrete. Yet, the exact mechanism of expansion and the role of gypsum and ettringite in the deterioration process remain subjects of controversy [1,4]. Santhanam [5] indicated the role of gypsum formation in the expansion and deterioration of cementitious matrices under external sulfate attack. Brown and Taylor [6] reviewed the mechanisms (topochemical growth, through-solution reactions, oriented crystal growth, etc.) by which ettringite can cause disruptive pressures in cement-based materials.

Migration of sulfate ions into concrete has been reported to cause the following chemical reactions:

$$SO_4^{-2} + Ca^{2+} + 2H_2O \rightarrow CaSO_4 \cdot 2H_2O \quad (1)$$

$$SO_4^{-2} + 2Ca^{2+} + Ca_4Al_2(OH)_{12} \cdot SO_4 \cdot 6H_2O \rightarrow Ca_6Al_2(OH)_{12}(SO_4)_3 \cdot 26H_2O \quad (2)$$

The above equations indicate the possible decomposition of CH and C–S–H leading to softening along with expansion. Hydroxyl ions (OH^-) may leach away to the surrounding solution resulting in a pH increase. In the case of alkali sulfates, alkali ions such as Na^+ can migrate to the pore solution, which increases the risk of alkali-aggregate reaction. Hydrated pozzolanic pastes with limited portlandite content and sulfate resistant cements with low C_3A content (less than 8%) have a high resistance, but are not completely immune to alkali sulfates [1,4].

If carbonates/bicarbonates are available in the cementitious matrix with abundance of moisture and a prevailing low temperature (less

* Corresponding author. Tel.: +1 519 661 2111x88308; fax: +1 519 661 3779.
E-mail address: mnehdi@eng.uwo.ca (M.L. Nehdi).

0008-8846/$ – see front matter © 2008 Elsevier Ltd. All rights reserved.
doi:10.1016/j.cemconres.2008.12.003

than 15 °C), thaumasite ($C_3S\overline{S}\,\overline{C}H_{15}$) can readily form and eventually lead to thaumasite sulfate attack (TSA) [7]. Thaumasite has been reported to form directly from C–S–H [1]:

$$SO_4^{-2} + 3Ca^{2+} + 3CO_3^{-2} + 3SiO_3^{-2} + 15H_2O \rightarrow 3CaO\cdot SiO_2\cdot CO_2\cdot SO_3\cdot 15H_2O \quad (3)$$

Progressive replacement of C–S–H with thaumasite usually produces a pulpy mass with non-binding characteristics. Numerous cases of this special form of sulfate attack have been reported since the last decade [e.g. [7–9]].

2. Need for research

Despite the current knowledge on, and standard specifications for concrete under sulfate attack, numerous cases of premature failure and costly rehabilitation of concrete structures exposed to sulfate environments have been reported [1,10]. There has often been different performance of concrete in classical sulfate immersion tests from that observed in field exposure mainly due to overlooking some important parameters existing in the field which accompany sulfate attack, such as the pH level and wetting–drying cycles [1,10,11]. On the other hand, the ongoing international shift to performance-based standards and specifications for concrete demands the development of new testing approaches that better correlate to service conditions. Such approaches can be particularly effective in evaluating emerging types of concrete such as self-consolidating concrete (SCC).

SCC readily flows and consolidates under its own weight with little or no vibration, which makes it suitable for precast applications, hard-to-reach areas and heavily reinforced sections. The mixture design of SCC usually incorporates an efficient superplasticizer, possibly a viscosity-modifying admixture, relatively high amounts of fine materials, relatively low water-to-powder ratio, and controlled proportions of coarse aggregates with adequate particle size and gradation [12,13]. Due to the difference in mixture design, placement and consolidation techniques, the durability of SCC may be different than that of normal concrete, and thus needs thorough investigation [14]. In a recent publication, Boel et al. [15] emphasized that essential knowledge on the durability of SCC is still needed before its safe use in various applications. The mixture design of SCC involves many variables such as limiting the coarse aggregate volume fraction, and the use of composite cements with a considerably larger volume fraction of supplementary cementitious materials (SCMs) and/or microfillers. In particular, the larger powder content (400–600 kg/m^3) and volume of cementitious paste (34–40%) of SCC [12,13] can make it particularly vulnerable to chemical attack, for example by sulfate solutions. Since the last decade, SCC has been widely used in areas vulnerable to sulfate attack such as substructures, industrial floors, infrastructure, etc. Previous studies on sulfate attack of SCC [e.g. [16,17]], used classical immersion tests, which might not correlate well with field conditions.

In real field exposure, the damage of concrete structures often occurs due to a multitude of mechanisms (chemical, physical and structural) acting in a combined and possibly synergistic manner. Thus, there is a need to develop performance tests that mobilize multiple damage mechanisms to improve the understanding of their combined effects on normal and emerging concretes, and hence allow a better modelling of the life-cycle performance of structures. Indeed, much research has been conducted on the deterioration of cement-based materials under external sulfate attack. However, little research has been done on the combined effects of external sulfate attack with other damage mechanisms. Such combinations are more relevant to in-service conditions than classical sulfate immersion tests. For instance, Miao et al. [18] investigated the combined effect of sodium sulfate and rapid frost action on non-air-entrained fibre-reinforced concrete using the ASTM C 666 test procedure A, except that 5% sodium sulfate was used instead of water. The study revealed the superior performance (in terms of the elastic dynamic modulus) of fibre-reinforced concrete specimens compared to that of plain concrete under dual damage mechanisms. In a series of studies [e.g. [19–21]], Schneider and coworkers indicated the vulnerability of cement-based materials to stress-corrosion. They investigated the degradation of mechanical properties (compressive and flexural strength) of mortar/concrete under sustained load and chemical attack (ammonium sulfate, sodium sulfate, sodium chloride and ammonium nitrate). It was concluded that stress is an influential factor affecting the rate of degradation of cement-based materials exposed to chemical attack depending on the level of applied stress [19–21].

In comparison to a reference full-immersion exposure, the present study investigates the durability of a wide range of SCC mixtures incorporating single, binary (two-component), ternary (three-component) and quaternary (four-component) binders, with and without hybrid fibre reinforcement to sulfate attack using a holistic testing regime, which also takes into account physical (cyclic environmental conditions) and structural (flexural stress) effects. The role of the coarse aggregate volume fraction (a key parameter in the mixture design of SCC controlling its rheology) and air-entrainment were also explored. The choice of the mixture design parameters was based on aspects related to the characteristic fresh properties and rheology of SCC. In addition to their effects on the fresh state of SCC, it is of equal importance to investigate whether these parameters affect the durability of SCC, particularly under simulated field-like conditions. The study should provide global data on the performance of these mixtures under such severe combined exposure and contribute to the needed shift to performance-based standards and durability-based design of concrete structures.

3. Experimental program

3.1. Materials

Twenty one SCC mixtures with a water-to-cementitious materials ratio (w/cm) of 0.38 were prepared using single, binary, ternary and quaternary binders. The mixtures were divided into three groups: group A (non-air-entrained SCC with a sand-to-total aggregates mass ratio [S/A] of 50%); group B (air-entrained SCC mixtures with S/A of 40 and 60%); and group C (air-entrained SCC with fibre reinforcement and sand-to-total aggregates plus fibres mass ratio of 50%). The binders used included CSA Type 10 (ASTM Type I) ordinary portland cement (OPC), CSA Type 50 (ASTM Type V) sulfate resistant portland cement (SRPC), silica fume (SF), Class F fly ash (FA), slag (S), and limestone filler (LF). Details of the chemical and physical properties of the various binders are listed in Table 1. Single binders were 100% OPC (control; designated codes A1, B1 or C1) or 100% SRPC (designated

Table 1
Chemical and physical properties of cement and SCMs

	OPC	SRPC	Silica fume	Fly ash	Slag	Limestone filler
SiO_2 (%)	19.8	22.3	94.0	48.9	35.0	0.3
CaO (%)	63.2	63.8	0.4	3.8	36.1	–
Al_2O_3 (%)	5.0	3.5	0.1	23.3	11.2	–
Fe_2O_3 (%)	2.4	4.0	0.1	14.9	0.5	–
MgO (%)	3.3	2.8	0.4	0.7	11.4	–
K_2O (%)	1.2	0.4	0.9	1.7	0.5	–
SO_3 (%)	3.0	2.1	1.3	0.2	3.3	–
Na_2O (%)	0.1	0.1	0.1	0.6	0.5	–
TiO_2 (%)	0.3	–	0.3	–	0.6	–
$CaCO_3$ (%)	–	–	–	–	–	99.0
Loss on ignition (%)	2.5	0.9	4.7	0.3	–	–
Specific surface area (m^2/kg)	410	377	19,530	280	468	3200
Specific gravity	3.17	3.15	2.12	2.08	2.90	2.70
C_3S[a]	61	54	–	–	–	–
C_2S	11	23	–	–	–	–
C_3A	9	1	–	–	–	–
C_4AF	7	14	–	–	–	–

[a]No correction has been made for possible use of limestone filler.

Table 2a
Proportions of binders per cubic meter of concrete

Binder description	Binder code	Cement kg	Silica fume kg	Slag kg	Fly ash kg	Limestone kg
100% SRPC	SRPC	470	–	–	–	–
100% OPC	A1, B1 or C1	470	–	–	–	–
92% OPC, 8% SF	A2, B2 or C2	430	40	–	–	–
50% OPC, 5% SF, 45% S	A3, B3 or C3	235	25	210	–	–
50% OPC, 15% LF, 20% S, 15% FA	A4, B4 or C4	235	–	95	70	70
50% OPC, 5% SF, 25% S, 20% FA	A5, B5 or C5	235	25	120	90	–

SRPC: sulfate resistant portland cement; OPC: ordinary portland cement; SF: silica fume; S: slag; LF: limestone filler; FA: fly ash.

code SRPC), binary binders contained 92% OPC and 8% SF (designated codes A2, B2 or C2), and ternary binders containing 50% OPC, 5% SF and 45% S (designated codes A3, B3 or C3). Quaternary binders comprised 50% OPC, 15% LF, 20% S and 15% FA (designated codes A4, B4 or C4), or 50% OPC, 5% SF, 25% S and 20% FA (designated codes A5, B5 or C5).

The total cementitious materials (binder) content was kept constant at 470 kg/m^3 to provide a relatively high volume fraction of fine materials (paste volume of 325–350 l/m^3), conforming to common SCC mixture design guidelines [12,13]. The fine aggregate was natural siliceous sand with a fineness modulus of 2.80, a saturated surface dry specific gravity of 2.65 and water absorption of 1.5%. Crushed stone (mostly siliceous gravel with a fraction of limestone aggregate) with a maximum nominal size of 19 mm, a saturated surface dry specific gravity of 2.68 and water absorption of 0.8% was also used. A polycarboxylate-based high-range water-reducing admixture (HRWRA) and a viscosity-modifying admixture (VMA) based on a solution of modified polysaccharide were used to enhance the flowability and stability of the SCC mixtures. The dosages of HRWRA and VMA were adjusted to maintain a slump flow of 650±30 mm and L-box (3 Ø10 mm bars with 50 mm gaps) ratio (H_2/H_1) not less than 0.70 for all mixtures. A multi-component synthetic air-entraining admixture (AEA) was used in groups B and C mixtures to obtain a fresh air content of 5±1%.

Table 2b
Proportions of groups A, B and C mixtures per cubic meter of concrete

Binder code	Mix. ID	Steel fibres (kg)	Polypropylene fibres (kg)	Fine aggregate (Kg)	Coarse Aggregate (kg)	Air-entraining agent (ml /100 kg of binder)
Group A						
SRPC	SRPC	–	–	870	870	–
A1	A1-N-50	–	–	870	870	–
A2	A2-N-50	–	–	860	860	–
A3	A3-N-50	–	–	855	855	–
A4	A4-N-50	–	–	845	845	–
A5	A5-N-50	–	–	840	840	–
Group B						
B1	B1-A-40	–	–	655	1015	45
	B1-A-60	–	–	1015	655	35
B2	B2-A-40	–	–	640	990	70
	B2-A-60	–	–	990	640	50
B3	B3-A-40	–	–	640	985	70
	B3-A-60	–	–	985	640	60
B4	B4-A-40	–	–	625	970	110
	B4-A-60	–	–	970	625	95
B5	B5-A-40	–	–	625	965	120
	B5-A-60	–	–	965	625	100
Group C						
C1	C1-A-H	30	1	830	805	40
C2	C2-A-H	30	1	825	795	60
C3	C3-A-H	30	1	820	790	65
C4	C4-A-H	30	1	805	780	100
C5	C5-A-H	30	1	800	775	105

In group C mixtures, micro-reinforcement of polypropylene fibrillated fibres with a specific gravity of 0.91 and graded length were added at a single dosage of 0.1% by volume. In addition, macro-reinforcement of crimped steel fibres with a specific gravity of 7.85, length of 38 mm, aspect ratio of 34, and tensile strength of 966–1242 MPa were used at a dosage of 0.4% by volume. Based on trial mixtures, these fibre shapes, lengths, and low volumes of micro- and macro-fibre reinforcement have proven adequate for achieving the characteristic flowability and passing ability of SCC with minimal clustering of fibres.

3.2. Experimental procedures

Constituent materials were mixed in a mechanical mixer in accordance to ASTM C 192 (Standard Practice for Making and Curing Concrete Test Specimens in the Laboratory). Tables 2a and 2b show the proportions of the tested SCC mixtures. For each mixture, eighteen replicates of 75×75×285 mm concrete prisms were prepared without compaction. Three replicates were used in the reference full-immersion test, and another three replicates were used for the combined exposure test without sustained flexural loading. The remaining twelve prism replicates were used in the combined exposure with sustained flexural loading (six prism replicates for the 25 and 50% stress levels, respectively). All specimens were demolded after 24 h and moist cured at 20 °C and 95% RH for 56 days. The hardened concrete properties of all mixtures at 56 days (before exposure) are listed in Table 3. To evaluate the durability of the tested SCC mixtures to sulfate attack, a reference exposure similar to that of ASTM C 1012 [22] (Standard Test Method for Length Change of Hydraulic-Cement Mortars Exposed to a Sulfate Solution) was used in which specimens were fully immersed in a 5% sodium sulfate solution up to 24 months. The temperature of the solution was maintained at around

Table 3
Hardened properties of groups A, B and C specimens at 56 days

Binder code	Mix. ID	Unit weight (kg/m^3)	Compressive strength (MPa)	Flexural strength (MPa)	E_d (GPa)
Group A					
SRPC	SRPC	2383	43.69	5.20	43.80
A1	A1-N-50	2371	47.12	4.99	45.40
A2	A2-N-50	2388	54.60	5.06	44.02
A3	A3-N-50	2365	50.18	4.40	41.38
A4	A4-N-50	2351	41.71	3.91	41.08
A5	A5-N-50	2335	46.78	4.20	40.04
Group B					
B1	B1-A-40	2291	38.91	4.41	41.25
	B1-A-60	2269	35.16	4.05	37.02
B2	B2-A-40	2284	43.64	4.23	40.94
	B2-A-60	2267	41.43	4.18	39.20
B3	B3-A-40	2253	39.56	3.76	34.37
	B3-A-60	2246	36.23	3.91	36.95
B4	B4-A-40	2259	32.34	3.61	35.07
	B4-A-60	2239	31.18	3.43	33.01
B5	B5-A-40	2218	34.23	3.50	34.04
	B5-A-60	2213	32.39	3.32	36.14
Group C					
C1	C1-A-H	2290	37.44	4.70	39.13
C2	C2-A-H	2297	42.34	4.65	39.95
C3	C3-A-H	2276	39.86	4.22	35.86
C4	C4-A-H	2264	33.41	3.74	36.64
C5	C5-A-H	2237	36.71	4.08	35.12

Notes
SRPC: 100% sulfate resistant Portland cement.
A1,B1, or C1: 100% OPC.
A2, B2, or C2: 92% OPC + 8% SF.
A3, B3, or C3: 50% OPC + 5% SF + 45% S.
A4, B4, or C4: 50% OPC + 15% LF + 20% S + 15% FA.
A5, B5, or C5: 50% OPC + 5% SF + 25% S + 20% FA.
N: non air-entrained, A: air-entrained.
50, 40, 60: S/A is 50, 40 and 60%, respectively.
H: hybrid fibres.

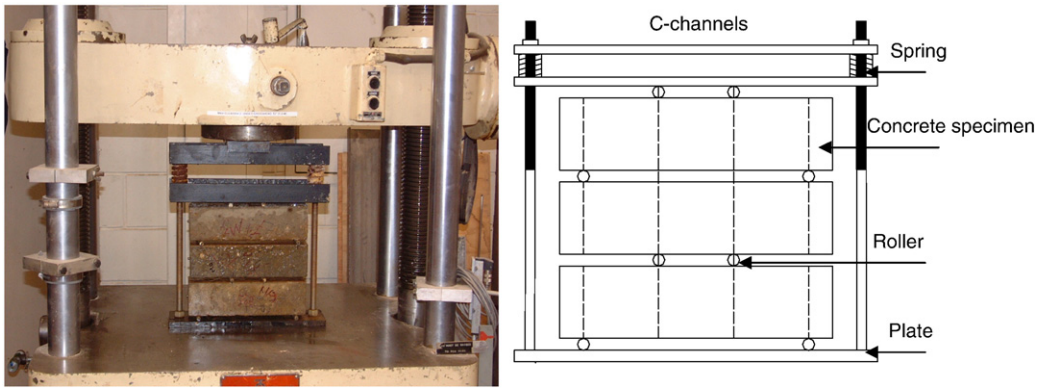

Fig. 1. Sustaining flexural stress on SCC specimens using steel frames with dual springs.

20±2 °C. The solution was renewed each 18 weeks, and the pH was controlled within a range of 6.0–8.0 by titration with diluted sulfuric acid solutions at regular time intervals (5 days). While controlling the pH of the sulfate solution is not specified in the ASTM C 1012, the importance of a controlled pH (6.0–8.0) of the sulfate solution correlates to field conditions in which concrete exists in a neutral environment with continual supply of sulfate ions [1,11].

In a second (combined) exposure, SCC specimens from the same mixtures were subjected to combined damages of sodium sulfate, cyclic environmental conditions and sustained flexural stress. This combination replicates field conditions for mechanically loaded concrete elements in sulfate-rich environments under seasonal climatic changes (consecutive cold winters and hot summers). Prismatic specimens from the SCC mixtures were subjected to stress ratios of 25 and 50% of their ultimate flexural strength (combined exposure with flexural loading). Flexural stress was mechanically applied to the specimens in four-point bending, and sustained using steel frames with dual springs (Fig. 1). These stress levels were maintained till the end of exposure. Comparatively, companion specimens were exposed to sulfate attack and cyclic environmental conditions without flexural stress (combined exposure without loading). Throughout the text, the two conditions of combined exposure with and without flexural loading are referred to as combined exposure (*F*) and combined exposure (*N*), respectively. When reference is made to both cases, the general term combined exposure is used.

Specimens with and without sustained flexural stress were initially immersed for 5 days in a 5% sodium sulfate solution (pH of 6.0–8.0) at a temperature of 20±2 °C before being exposed to the cyclic environmental conditions that simulated successive winter and summer seasons. A winter season (Fig. 2a) was represented by 30 successive freezing–thawing cycles: freezing in air at −18±1 °C for 12 h followed by thawing in a 5% sodium sulfate solution (pH of 6.0–8.0) at 5±1 °C for 6 h, 4 h to ramp to the minimum freezing temperature, and 2 h to ramp to the maximum thawing temperature. A summer season comprised 7 to 8 alternating wetting–drying cycles. Each cycle consisted of 2 days of immersion in a 5% sodium sulfate solution (pH 6.0–8.0) at a temperature of 20±2 °C followed by 2 days of drying at 40 °C and 40% RH (Fig. 2b). The experiment was conducted in a sate-of-the-art walk-in environmental chamber with automated temperature and RH controls. The solution was renewed every 30 days (season) and pH control was done similar to the reference exposure. The experiment lasted for one year, simulating 6 winters alternating with 6 summers under sustained flexural loading and sulfate attack.

The selection of the temperature extremes in the combined exposure is comparable to that in various geographic locations in North America, while the application of long freezing periods also correlates to outdoor exposures in northern climates [23]. Yet, the aforementioned combination of aggressive factors (high concentration of sodium sulfate and levels of flexural stress with alternating freezing–thawing and wetting–drying cycles) can cause more severe damage of SCC than that under actual field conditions. Indeed, this test procedure is considered accelerated aiming to obtain results that relatively correspond to field performance under harsh conditions within a reasonable laboratory testing time span.

Before exposure, the initial physico-mechanical properties of the intact specimens were measured. For all specimens, the initial mass, length (ASTM C 1012), dynamic modulus of elasticity, E_d (ASTM C 215 [24] Standard Test Method for Fundamental Transverse Resonant Frequency of Concrete Specimens, calculated as the square of the fundamental transverse frequency according to the ASTM C 666 guidelines), and flexural strength (ASTM C 78 Standard Test Method for Flexural Strength of Concrete Using Simple Beam with Third-Point Loading [25]) were recorded. Specimens were removed from the sulfate solutions at specified time intervals, and the free expansion of prisms (only for specimens in the reference exposure and the ones in the combined exposure N) was immediately measured. Subsequently,

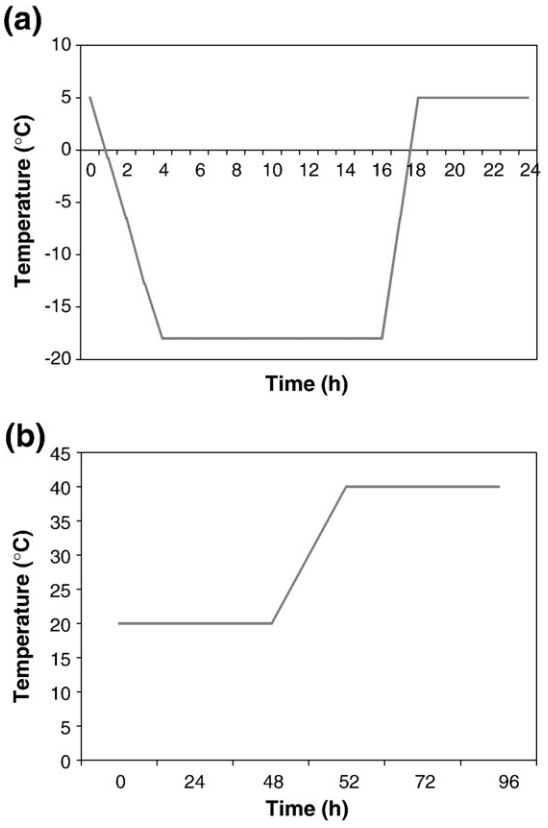

Fig. 2. Temperature profile for: (a) a freezing–thawing cycle, and (b) a wetting–drying cycle.

debris, if any, were removed by a nylon brush, and the specimens were left to dry under 20 °C and 50% RH for 30 min before visual inspection and measurement of mass and fundamental transverse frequency. Relative to the initial values, the change in mass, length and dynamic modulus of elasticity (RE_d) versus time of exposure, and the change in flexural strength (RF) at the end of the combined exposure were calculated. The measurements of expansion and RE_d were made every 30 days (season).

To analyse the sulfate reaction phases, differential scanning calorimetry (DSC) was conducted on powder samples (particle size ≤40 μm) collected from the surface (0–15 mm depth from the exposed surface) of selected specimens. To complement the results obtained by DSC, X-ray diffraction (XRD, Cu-Kα) was conducted on identical powder samples. To assess deterioration in the microstructure, polished sections were prepared for optical microscopy analyses. The polished sections were prepared from fracture surfaces that were dried at 40 °C for 24 h, impregnated with low-viscosity epoxy resin under pressure, cut, and polished. Backscattered and secondary scanning electron microscopy (BSEM, SEM) with energy dispersive X-ray analysis (EDX) were also used on gold coated selected thin sections and fracture surfaces to supplement the findings of optical microscopy. In the case of loaded prism specimens, all thermal, mineralogical and microscopy analyses were conducted on samples collected from the tension face (unless otherwise indicated) in the middle-third span subjected to the maximum bending moment.

4. Results of exposure I: sodium sulfate attack

Table 4 lists the results of expansion, change in dynamic modulus of elasticity (RE_d) and mass change for the SCC specimens immersed in the sodium sulfate solution after 12 and 24 months of exposure. Up to 24 months of immersion, specimens had a relatively low expansion that did not exceed 0.06%. RE_d showed a small but consistent increase with time (maximum of 8%). The expansion and increase in RE_d were accompanied by a slight (about 1%) increase in the mass of specimens.

The ASTM C 1012 allows an expansion of up to 0.10% for smaller mortar bars having higher surface-to-volume ratio (compared to the concrete prisms used in the present study) and w/cm (0.485), after 12 months of immersion in a 5% sodium sulfate solution [22]. For mortar specimens made with blended binders and subjected to Class 3 sulfate exposure (more than 10,000 ppm SO_4^{-2}), ACI 201.2R (Guide to Durable Concrete) permits an expansion of up to 0.10% after 18 months of exposure following the ASTM C 1012 procedure [26]. The appendix of ASTM C 1012 indicates that the user may modify the test method to use other sulfate solutions, other ages/degrees of maturity, or other materials proportions [22]. However, the standard test does not specify controlling the pH of the used sulfate solution. It has been reported that the pH of the solution rises rapidly upon the immersion of mortar bars up to a value similar to that of the cementitious matrix (11.0–13.0), which decelerates the kinetics of deterioration [1,11,27]. Despite that the full-immersion procedure in the current study was conducted on concrete prisms of lower surface-to-volume ratio, the test environment was more aggressive than that of the ASTM C 1012 since the pH was constantly controlled at a neutral level (~7). Brown [27] reported that this pH level is more detrimental to specimens under sulfate attack than the uncontrolled conditions of the ASTM C 1012. The present results suggest that the rate of damage for the SCC specimens immersed in the sodium sulfate solutions was slow. Even after 24 months in a neutral pH environment, there was a general increase in mechanical properties due to continuous hydration of the matrix and filling of voids with reaction products as suggested by previous studies [e.g. [5,28]]. Despite the relatively high concentration of the sulfate solution (33,800 ppm of SO_4^{-2}) and its neutral pH level, specimens did not show any evidence of softening or significant expansion (not more than 0.06%) up to 24 months of exposure. Hence, all the SCC mixtures studied herein can be classified as sulfate resistant based on the full-immersion procedure.

Irrespective of the binder type, the mechanical properties of all tested specimens were not degraded after the full-immersion exposure. This behaviour can physically be correlated to the low penetrability of this type of high-performance concrete (w/cm 0.38, and high powder content) that is produced without vibration (homogenous microstructure). In addition, the results of mercury intrusion porosimetry (Fig. 3) conducted on unexposed companion specimens showed that the SCC specimens made from blended binders had lower cumulative intrusion and/or further pore size refinement relative to that of the control specimens prepared with 100% OPC, implying lower penetrability. Densification of the pore structure is attributed to the pozzolanic reaction and physical filler

Table 4
Results of expansion, relative dynamic elastic modulus (RE_d) and mass change for SCC specimens after the reference and combined exposures (N)

Mix. ID	Reference exposure						Combined exposure (no-loading), 12 months		
	12 months			24 months					
	Expansion (%)	RE_d (%)	Mass change (%)	Expansion (%)	RE_d (%)	Mass change (%)	Expansion (%)	RE_d (%)	Mass change (%)
Group A									
SRPC	0.02	109	0.62	0.02	106	0.62	0.13	110	0.76
A1-N-50	0.04	106	0.61	0.06	99	0.91	0.22	81	0.92
A2-N-50	0.02	107	0.65	0.03	101	0.82	0.12	103	−0.28
A3-N-50	0.01	107	0.63	0.02	103	0.55	0.20	82	−2.21
A4-N-50	0.02	109	0.57	0.04	104	0.37	0.33	46	2.65
A5-N-50	−0.01	108	0.23	0.01	99	0.37	0.25	57	0.56
Group B									
B1-A-40	0.02	107	1.01	0.05	104	1.31	0.21	90	1.16
B1-A-60	0.02	106	1.18	0.04	99	0.92	0.19	93	2.14
B2-A-40	0.02	107	0.88	0.03	99	1.23	0.20	95	0.49
B2-A-60	0.03	108	1.10	0.04	101	1.08	0.17	98	1.28
B3-A-40	0.01	109	1.00	0.03	102	1.51	0.18	106	1.18
B3-A-60	0.02	108	0.78	0.02	98	0.34	0.16	95	0.33
B4-A-40	0.02	109	0.38	0.04	101	0.78	0.23	83	−3.12
B4-A-60	0.02	107	0.36	0.03	103	0.44	0.16	97	0.17
B5-A-40	0.05	109	0.77	0.05	106	0.67	0.11	91	−1.21
B5-A-60	−0.01	109	0.76	0.01	101	0.91	0.16	108	2.89
Group C									
C1-A-H	0.03	107	0.96	0.05	102	1.21	0.20	83	−3.25
C2-A-H	0.02	106	1.03	0.03	108	0.58	0.21	81	4.37
C3-A-H	0.02	109	0.92	0.03	108	0.81	0.19	88	−2.64
C4-A-H	0.01	111	0.55	0.03	108	0.74	0.19	90	−1.65
C5-A-H	0.02	110	0.74	0.04	102	0.92	0.18	85	−3.10

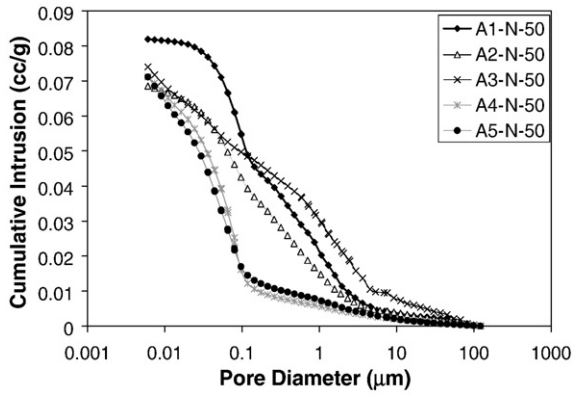

Fig. 3. Pore size distribution of SCC specimens at 56 days (before exposure) for group A mixtures.

effects of SCMs incorporated in blended binders. Results from the present study emphasize the significant role of using a w/cm of less than or equal to 0.40 to resist very severe sulfate exposure (more than 10,000 ppm SO_4^{-2}), as also addressed by ACI 201.2R [26].

On the other hand, the chemical resistance of the type of cementitious materials used, particularly those incorporating SCMs or containing SRPC may have contributed to discounting the rate of damage in the full-immersion exposure. While SRPC had a low C_3A content (1% – Table 1), blended binders used in this study were designed to reduce the CH content in the hydrated cementitious matrix, thus improving the resistance to alkali sulfates. From a mixture proportioning perspective, there is a dilution effect (reduction of C_3A content) in the cementitious paste especially at a high OPC replacement level (50%) in ternary and quaternary binder mixtures compared to only 8% in the binary mixture. SCMs react with CH and water to produce C–S–H (pozzolanic reaction). Increasing the replacement level of OPC by SCMs is inversely proportional to the amount of CH formed in the paste. This is depicted by the DSC results in Fig. 4, where enthalpies of CH (440 °C) for the ternary and quaternary binder mixtures were significantly lower than that of the binary and control mixtures. Thus, blended binder matrices with lower portlandite contents can reduce the potential for gypsum formation when exposed to alkali sulfates (Eq. (1)). Additionally, Skalny et al. [1] reported that cementitious systems incorporating SCMs tend to form hydrated alumina-bearing phases that are not vulnerable to sulfate attack, but such an effect was not quantified in the current study.

Since all tested specimens had comparably improved performance under the full-immersion exposure, it can be stated that the physical resistance (i.e. low penetrability) of SCC was more important than the chemical resistance of its binder in mitigating the kinetics of deterioration due to external sulfate attack.

Based on the performance of the SCC mixtures in the full-immersion exposure, they can qualify for use in severe exposure to alkali sulfates. Yet, whether those mixtures can maintain their performance when sustained loading and cyclic environmental conditions are involved, and what could be the mutual effects of combined damage on those cementitious matrices are aspects not captured by the full-immersion test, and thus need to be investigated.

5. Results of exposure II: combined exposure

5.1. Visual inspection

All specimens showed slight surface scaling on all faces, which was often accompanied by spalling along the edges and/or at the corners (Fig. 5a). By the end of exposure, some non-loaded specimens that had marked reduction in engineering properties (e.g. A4-N-50) had visible macro-cracks on the surface (Fig. 5b). Unlike the case of the reference full-immersion exposure, some loaded specimens suddenly failed by a typical flexural breakage at the middle-third span during the combined exposure (Fig. 5c). Comparatively, loaded SCC specimens comprising hybrid fibre reinforcement showed flexural cracking in the middle-third span, but without splitting into two-halves owing to the effect of fibres (Fig. 5d).

5.2. Expansion

The results of expansion for the non-mechanically loaded SCC specimens from groups A, B and C mixtures are listed in Table 4. By comparing those results with that of the reference exposure (immersion in 5% sodium sulfate solution at 20±2 °C – Table 4), the effect of cyclic environmental conditions on the sulfate resistance of the SCC specimens can be observed. After 12 months under the combined exposure (N), the expansion values of SCC specimens from groups A, B and C were significantly higher by average factors of 13, 10 and 10, respectively than that of the corresponding specimens in the reference full-immersion exposure. Unlike the results obtained from the reference exposure, all expansion values exceeded 0.1%. High expansion (more than 0.25%) was usually accompanied by a marked reduction in RE_d (up to 46%) and surface macro-cracks (e.g. Fig. 5b). This is in contrast to the reference exposure,

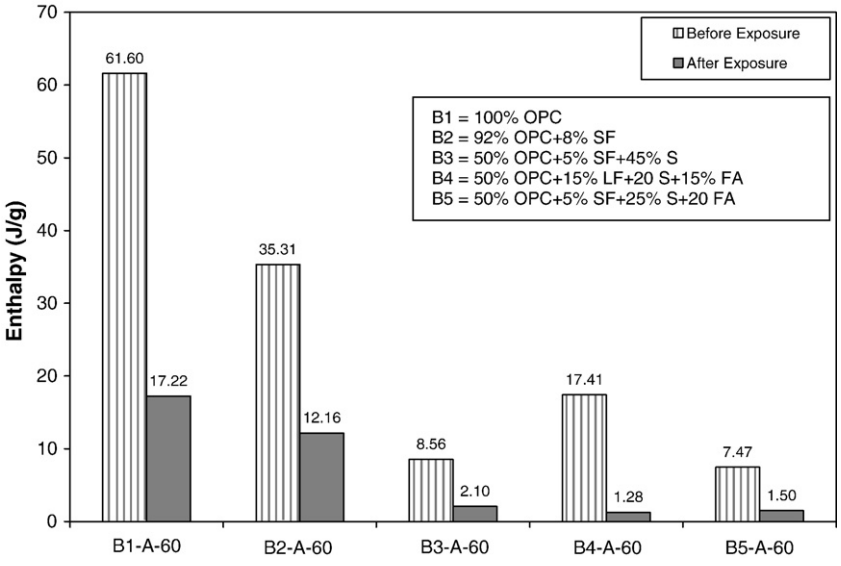

Fig. 4. DSC results for CH peaks at about 440 °C.

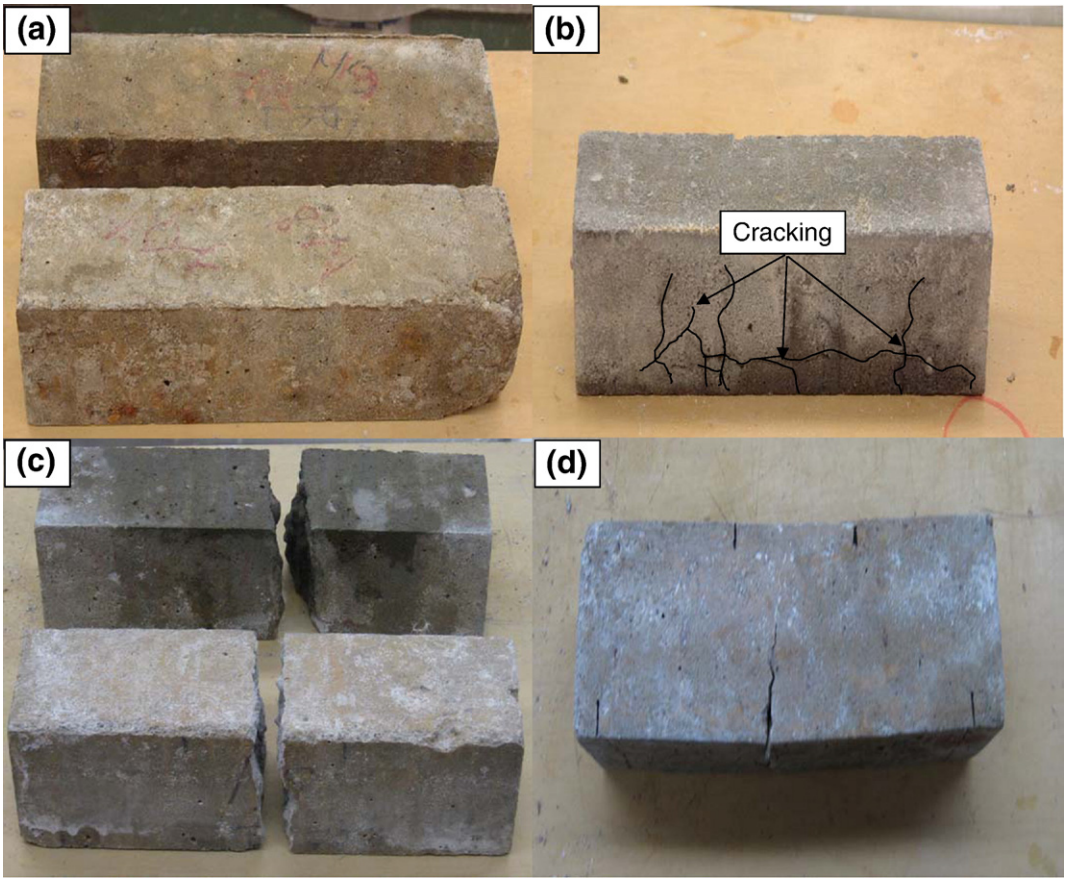

Fig. 5. Visual features for SCC specimens under the combined exposure: (a) surface scaling, (b) macro-cracks of a non-loaded specimen, (c) flexural breakage of loaded specimens, and (d) cracking of a loaded fibre-reinforced specimen.

where there was no evident reduction in RE_d for up to 24 months. Hence, the deterioration of SCC specimens was aggravated when combining cyclic environmental conditions (freezing–thawing and wetting–drying) with sulfate attack.

In group A, the analysis of variance (ANOVA) at a significance level α=0.05 showed that variation in the type of binder affected the mean of the expansion results since it had an F value of 32.12, which is larger than the corresponding critical F value of 4.38 (Table 5). According to Montgomery [29], exceeding the critical value of an F-distribution density function reflects that the tested variable affects the mean of the results. Specimens from the SRPC and binary binders yielded moderate expansion (0.13 and 0.12%, respectively), whereas the control (A1-N-50) specimens prepared with 100% OPC had a higher expansion of 0.22%. Specimens from the quaternary binder with limestone filler (A4-N-50) had the highest expansion of 0.33%, corresponding to inferior engineering (RE_d and RF) properties and surface macro-cracks. This is in large contrast with results of the reference full-immersion tests.

From Table 4, depending on the type of binder, air-entrainment in group B mixtures generally reduced the expansion of SCC specimens compared to that of the corresponding non-air-entrained specimens from group A. For example, specimens from the air-entrained ternary binder (B3-A-60) had 20% lower expansion than that of the corresponding non-air-entrained (A3-N-50) specimens made from the same ternary binder, which was 0.2%. The expansion values of specimens from the air-entrained quaternary binder with limestone filler (B4-A-40 and B4-A-60) were 70 and 48%, respectively, of the expansion value of the corresponding non-air-entrained (A4-N-50) specimens from group A, which yielded the highest expansion of 0.33%. ANOVA showed that variation in S/A did not affect the mean of the expansion results in group B since it had an F value of 0.86, which is smaller than the corresponding critical F value of 7.70 (Table 5).

The expansion values of group C specimens were all below the high threshold of 0.25%, and they were in the narrow range of 0.18–0.21%. Correspondingly, there was no significant decline in RE_d of these specimens (Table 4). ANOVA showed that variation in the type of binder did not affect the mean of the expansion results in group C since it had an F value of 1.19, which is smaller than the corresponding critical F value of 5.19 (Table 5). It seems that the incorporation of low volumes of hybrid fibres controlled the expansion behaviour of SCC specimens under the combined exposure (N), which probably masked the effect of the different binders.

5.3. Onset of failure

Despite the observed high expansion values (up to 0.33%), no single SCC specimen without sustained flexural stress failed (i.e. completely

Table 5
Typical ANOVA results for the combined exposure

Tested variable	Mixture group	Exposure	Measured property	F	$F_{critical}$	Statistical effect on mean results
Type of binder	A	Combined (N)	Expansion	32.12	4.38	Yes
Type of binder	C	Combined (N)	Expansion	1.19	5.19	No
Type of binder	A	Combined (N)	RE_d	14.21	3.32	Yes
S/A	B	Combined (N)	Expansion	0.86	7.70	No
Stress Level	A	Combined	RE_d	16.61	4.10	Yes
Stress Level	C	Combined	RE_d	11.78	4.15	Yes

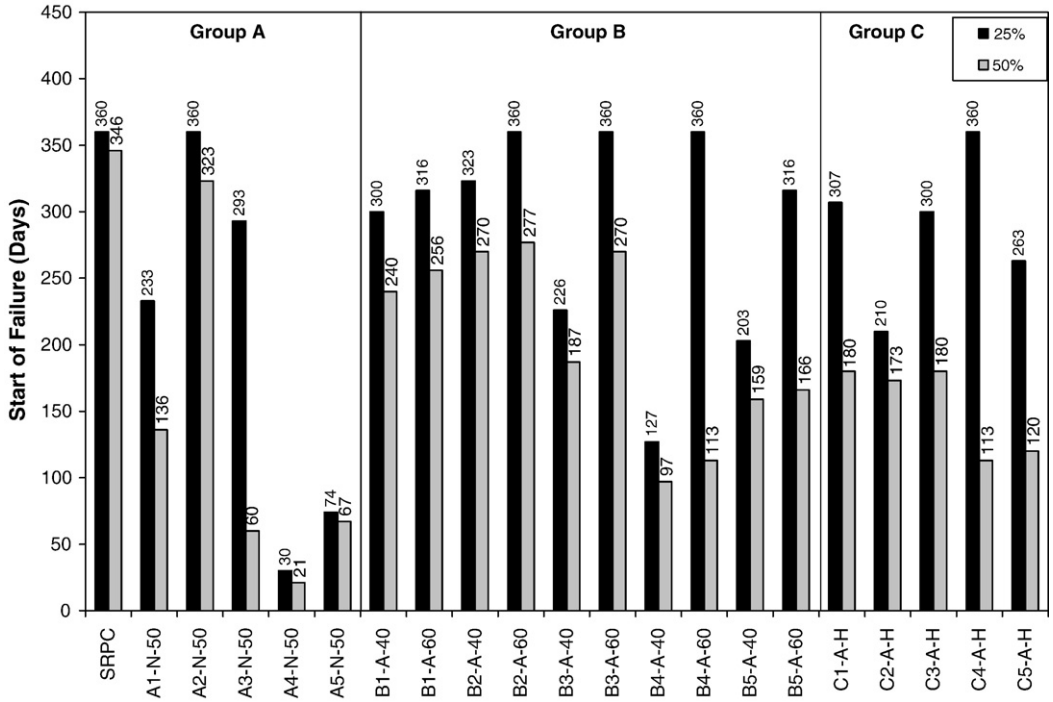

Note: Specimens from SCC mixtures with a designated value of 360 days did not fracture up to 360 days of combined exposure.

Fig. 6. Onset of breakage for SCC specimens exposed to the combined exposure: sulfate attack, cyclic environments and flexural loading.

lost its flexural capacity) due to transverse cracks. Conversely, loaded specimens started to fail spontaneously at stress levels of 25 and 50% of their ultimate flexural strength, except for those incorporating hybrid fibres, depending on the applied stress level. Failure of SCC specimens with hybrid fibres was indicated by the earliest visible macro-crack, approximately corresponding to the first-cracking stress (prior to the post-peak behaviour). Fig. 6 shows the time at which mechanical failure of SCC specimens under combined exposure (*F*) started. It can be noted that the majority of the SCC specimens were susceptible to stress corrosion as indicted by the sudden failure of specimens, particularly under the high flexural stress (50% of the ultimate strength). According to Schneider et al. [19–21] stress-corrosion is a chemo-mechanical phenomenon in which abrupt failure of materials occurs due to the exposure to a constant tensile stress and corrosive environment/chemical solutions. The propagation of cracks under such conditions is accelerated leading to sudden failure [19]. Fig. 6 illustrates that SCC specimens under a stress level of 50% generally failed earlier than similar specimens under a stress level of 25%. For example, specimens from the ternary binder (A3-N-50) started to fail after 60 and 293 days under the combined exposure (*F*) at stress levels of 50 and 25%, respectively.

Statistical analysis by ANOVA confirmed that variation of the applied stress from 0 to 50% significantly influenced the deterioration of engineering properties under the combined exposure. For instance, in groups A and C, ANOVA of the RE_d results showed that variation of the stress level had *F* values of 16.61 and 11.78, respectively, which are larger than the corresponding critical *F* values of 4.10 and 4.15 (Table 5). A similar trend was observed for the *RF* results. Therefore, the damage rate was further accelerated when a sustained flexural stress was combined with the chemical and physical (environmental) attacks.

5.4. Relative dynamic modulus of elasticity (RE_d)

The results of change in RE_d versus the time of combined exposure (*F*) under stress levels of 25 and 50% for groups A, B and C mixtures are shown in Figs. 7a–c and 8a–c, respectively. As mentioned earlier, some loaded specimens spontaneously failed during the combined exposure (*F*). This entailed the multiplication (correction) of mean results by the reliability of SCC mixtures at each time of measurement, where reliability is the complimentary to the probability of failure (P_f):

$$\text{Reliability} = 1 - P_f, \text{ and } P_f = \frac{\Sigma f}{n} \quad (4)$$

where, *f* and *n* are the cumulative number of failed specimens up to a certain point of time and the total number of specimens, respectively. Therefore, zero RE_d reflected the failure of all replicates of an SCC mixture. The purpose of reliability is to reflect whether some or all specimens failed under the sustained loading. For example, if three specimens failed, and the average RE_d for the remaining (unbroken) specimens were 80%, reporting the value of 80% would give a misleading indication that the mixture is performing well. However, if the RE_d value is corrected (multiplied) by the reliability of the mixture, a more realistic assessment of performance is achieved. In this case, the reliability is: 1−(3/6)=0.5 and the value of 80% will be corrected to 80*0.5=40%. Thus, this gives a more representative performance of the mixtures. This concept was used by Schneider and coworkers [e.g. [21]] in their studies on stress-corrosion of cement-based materials.

The type of binder also had a pronounced effect on the RE_d results. In group A, ANOVA of the RE_d results showed that variation of the type of binder had an *F* value of 14.21, which is larger than the corresponding critical *F* value of 3.32 (Table 5). Similar trends were observed for specimens made with different binders under stress levels of 0, 25 and 50%. For example, at the end (360 days) of the combined exposure (F) and under a stress level of 25%, the control (A1-N-50) specimens failed the 60% RE_d threshold recommended by the ASTM C 666 guidelines for durable concrete subjected to freezing–thawing cycles. Conversely, SRPC specimens from mixtures prepared with 100% sulfate resistant portland cement maintained a high RE_d

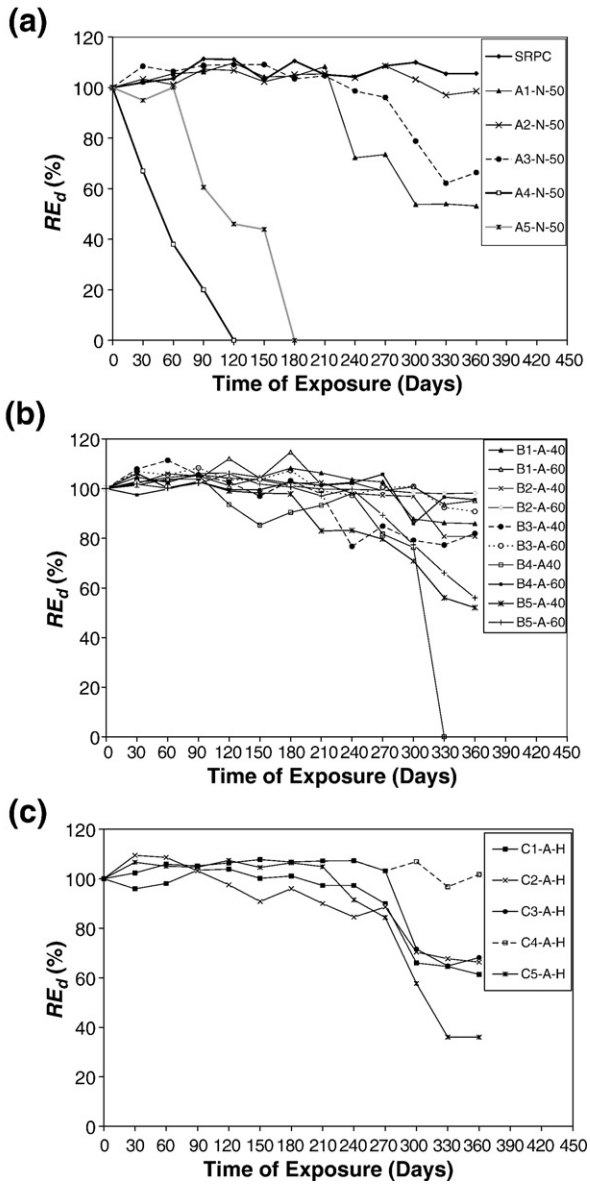

Fig. 7. Relative dynamic modulus of elasticity vs. the time of exposure for groups (a) A, (b) B, and (c) C specimens under a stress level of 25%.Notes: Corrected by the reliability of each mixture based on the number of failed specimens.

above 100% over the time of exposure. At the end of the combined exposure (*F*) and under a stress level of 25%, specimens from the binary (A2-N-50) and ternary (A3-N-50) binders did not fail the 60% l RE_d limit (Fig. 7a) with RE_d values of 98 and 67%, respectively. In contrast, specimens from the quaternary binders failed the 60% RE_d limit at early stages. Specimens from the quaternary binders (A4-N-50) made with 50% OPC, 15% LF, 20% S and 15% FA, and (A5-N-50) made with 50% OPC, 5% SF, 25% S and 20% FA, started to fail after 30 and 74 days of exposure (Fig. 6), respectively, and completely failed (zero RE_d) by 120 and 180 days, respectively (Fig. 7a). Likewise, non-loaded specimens from those quaternary binders had significant expansion and a marked drop in RE_d after 360 days of combined exposure (*N*) (Table 4). Similar to the trends observed in group A, the specimens from the quaternary binder mixture incorporating 50% OPC, 15% LF, 20% S and 15% FA in group B had inferior performance under the combined exposure (F). For instance, the (B4-A-40) specimens failed prior to the other specimens and had zero RE_d by 330 and 210 days of combined exposure (*F*) under stress levels of 25 and 50%, respectively (Figs. 7b and 8b).

In agreement with the expansion results of non-loaded specimens, RE_d results suggested that air-entrained SCC specimens from group B mixtures generally performed better and/or survived longer under the combined exposure (*F*) than the corresponding non-air-entrained SCC specimens from group A mixtures. From Table 4, RE_d results of non-loaded SCC specimens under the combined exposure (*N*) were well above the failure limit of 60% (83 to 108%). At a stress level of 25%, no SCC specimen had a drop in RE_d below 60% prior to 300 days of exposure (Fig. 7b). At a stress level of 50%, except for the specimens from the quaternary binder with limestone filler (B4-A-40 and B4-A-60), no other specimen fell short of the 60% limit before 200 days of exposure (Fig. 8b). Again, the effect of the S/A on the RE_d results was not clear. At all stress levels, ANOVA of the RE_d results showed that variation of S/A had *F* values less than the corresponding critical ones.

Under stress levels of 0, 25 and 50%, RE_d results for group C mixtures were in the ranges of 81 to 90% (Table 4), 36 to 102% (Fig. 7c) and 0 to 57% (Fig. 8c), respectively, indicating that variation in the stress level had a significant effect on the RE_d results. While non-

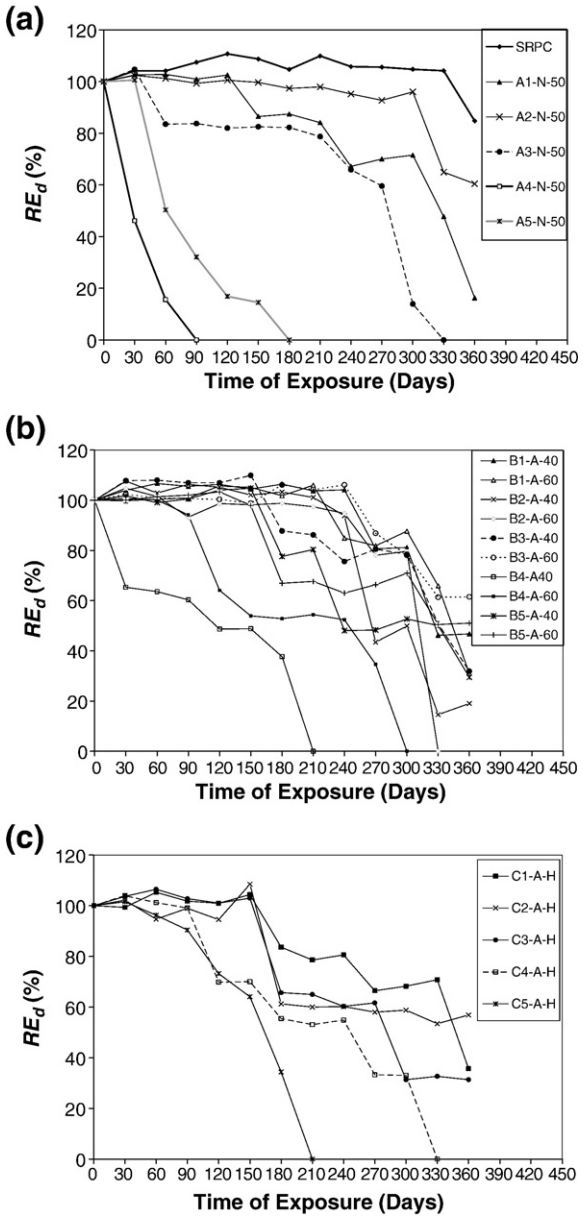

Fig. 8. Relative dynamic modulus of elasticity vs. the time of exposure for groups (a) A, (b) B, and (c) C specimens under a stress level of 50%. Notes: Corrected by the reliability of each mixture based on the number of failed specimens.

Table 6
Relative flexural strength (*RF*, %) of SCC specimens at the end of the combined exposure

Mix. ID	Stress ratio		
	0	25[a]	50[a]
Group A			
SRPC	113	109	88
A1-N-50	86	60	21
A2-N-50	115	62	22
A3-N-50	85	40	–
A4-N-50	25	–	–
A5-N-50	53	–	–
Group B			
B1-A-40	100	104	37
B1-A-60	94	83	50
B2-A-40	80	46	7
B2-A-60	113	108	–
B3-A-40	98	67	7
B3-A-60	88	90	38
B4-A-40	48	–	–
B4-A-60	112	73	–
B5-A-40	83	48	9
B5-A-60	96	68	53
Group C			
C1-A-H	40	57	16
C2-A-H	42	53	57
C3-A-H	61	58	19
C4-A-H	85	76	–
C5-A-H	59	41	–

[a] Corrected by the reliability of each mixture based on the number of failed specimens.

loaded air-entrained SCC specimens with hybrid fibre reinforcement notably passed the 60% RE_d limit at the end of the combined exposure (N) (Table 4), they failed this limit under the combined exposure involving a high stress level of 50%. In addition, the specimens from the quaternary binders with or without limestone filler (C4-A-H and C5-A-H) completely failed by 330 and 210 days of exposure under the 50% stress level. Fig. 6 shows that SCC specimens with hybrid fibres started to fail at a stress level of 50% earlier than corresponding specimens from groups A and/or B (e.g. compare C2-A-H (173 days) to A2-N-50 (323 days) and B2-A-40 (270 days)/B2-A-60 (277 days) at a stress level of 50%). This implies that the incorporation of low volumes of hybrid fibres adversely affected the performance of SCC specimens under the combined exposure of sulfate attack, cyclic environments and flexural loading, particularly at the high flexural stress level.

5.5. Relative flexural (RF) strength

Average results of the relative flexural strength (*RF*) at the end of the combined exposure are listed in Table 6. Such results were corrected by the reliability of each SCC mixture similar to the RE_d results. Contrary to the reference full-immersion exposure, there was an evidence of flexural strength loss. Despite that all non-loaded specimens survived the entire length of exposure, a marked drop in *RF* (up to 25%) was observed (Table 6). Loaded specimens started to fail during exposure, and some SCC mixtures completely failed before the end of exposure (e.g. [A4-N-50 and B4-A-40] specimens). In all groups, there was a general trend of reduction in *RF* with an increase of the stress level (Table 6). For example, specimens from the quaternary binder without limestone filler (B5-A-60) had *RF* values of 96, 68 and 53% under stress levels of 0, 25 and 50%, respectively.

Generally, *RF* results (with a few discrepancies) agreed well with the observed trend of RE_d results under all stress levels, confirming the internal deterioration of specimens. As shown in Fig. 9, there is a quadratic relationship between the two parameters with a coefficient of determination R^2 of 0.87. This relationship is qualitative showing the consistency of results, where the two parameters exhibited comparable trends. The selection of a quadratic relationship was based on regression analysis, where other relationships, e.g. linear, exponential, etc. yielded lower R^2 values. An *RF* of 50% corresponded to RE_d of less than 60%. Such an observation can be used in establishing performance testing based on multiple damage mechanisms.

Table 6 shows that many SCC specimens comprising hybrid fibre reinforcement (group C) had notable reduction in *RF*, especially at high stress level. This reduction was comparable or greater than that of the corresponding non fibre-reinforced specimens from groups A and/or B. For instance, at a stress level of 25%, the loaded control (C1-A-H) specimens with hybrid fibre reinforcement had an *RF* of 57% compared to an *RF* of 60% for the corresponding control (A1-N-50) specimens without fibre reinforcement.

5.6. Mass change

Unlike expansion, RE_d and *RF* results, the mass change results for the SCC mixtures did not show distinctive trends. Moreover, variation in the stress level did not affect the results of mass change. Fig. 10 shows an example of mass change for SCC specimens from group A mixtures under the combined exposure (*F*) at a stress level of 25%.

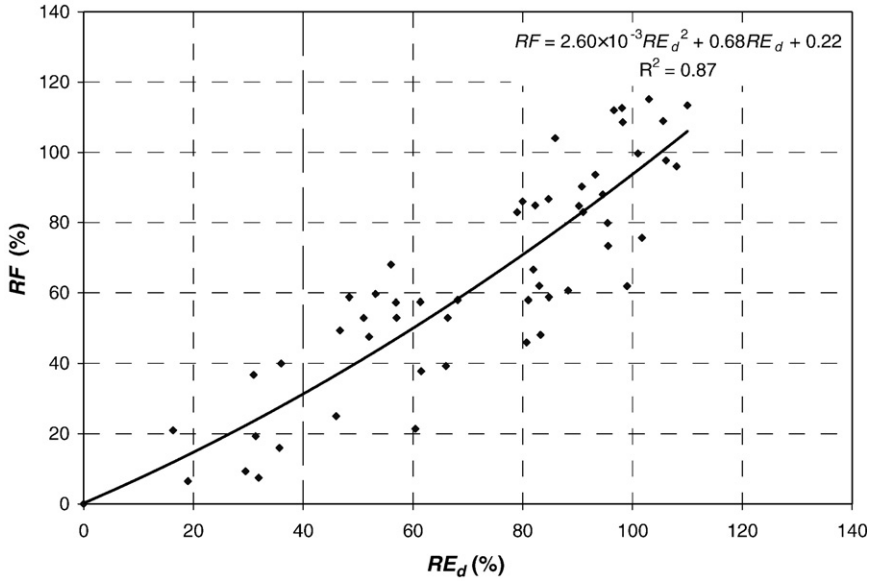

Fig. 9. Relationship between relative dynamic modulus of elasticity and relative flexural strength after the combined exposure.

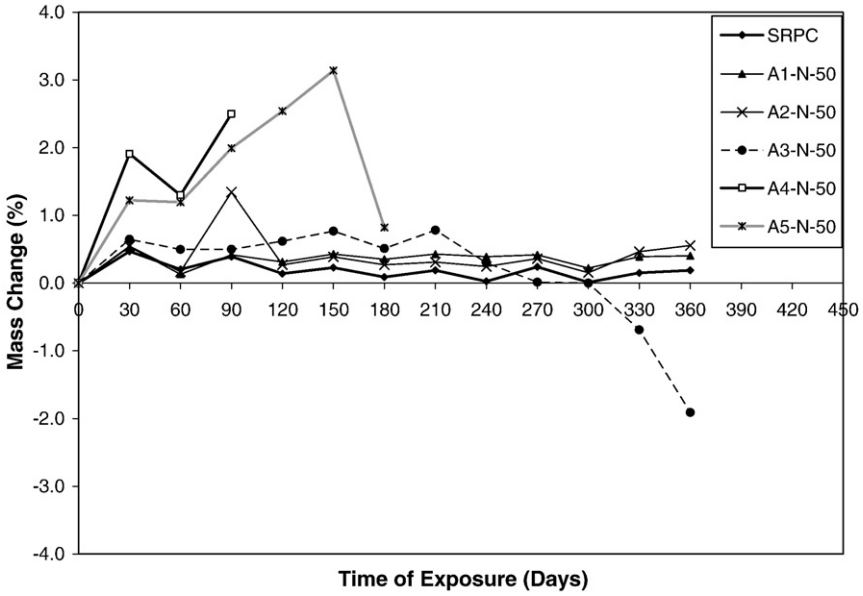

Fig. 10. Mass change of group A specimens vs. the time of exposure (stress level=25%).

Despite the observed surface scaling on all specimens, some SCC specimens had slight mass gain over their respective time of exposure. Others initially had a slight gain in mass followed by a decreasing trend at later stages of the test. The final mass for some specimens was slightly lower than the corresponding initial value before exposure (maximum mass loss of 3%), but no severe mass loss was observed. Specimens that lost mass did not necessarily suffer significant reduction in engineering properties.

6. Discussion

The mechanisms and rate of deterioration under the combined exposure were different from that of the reference full-immersion exposure due to the mutual and coupled effects of sulfate attack, environmental conditions and flexural stress. Although all the SCC mixtures could qualify as durable for a 'very severe' alkali sulfate exposure based on the full-immersion test, some of these mixtures failed to maintain their engineering properties under the combined exposure, and even some failed at early stages of the test. Negligence of such combined effects partially explains why the commonly used full-immersion sulfate attack tests have frequently shown variable performance from that observed under field exposure.

6.1. Effect of binder type

DSC analyses on powder samples collected from the surface of selected specimens made with various binders (from group B mixtures) showed notable reduction in the CH enthalpies relative to their initial values determined before the combined exposure (Fig. 4). This suggests that the tested binders were susceptible to sulfate attack reactions under the combined exposure, though with varying degrees. The consumption of CH in sulfate chemical reactions produces deleterious sulfate-bearing compounds of gypsum and ettringite, and sometimes thaumasite (Eqs. (1)–(3)). These crystalline products may coexist in degraded cementitious matrices exposed to sulfate attack. The DSC peaks of ettringite, thaumasite and gypsum are known

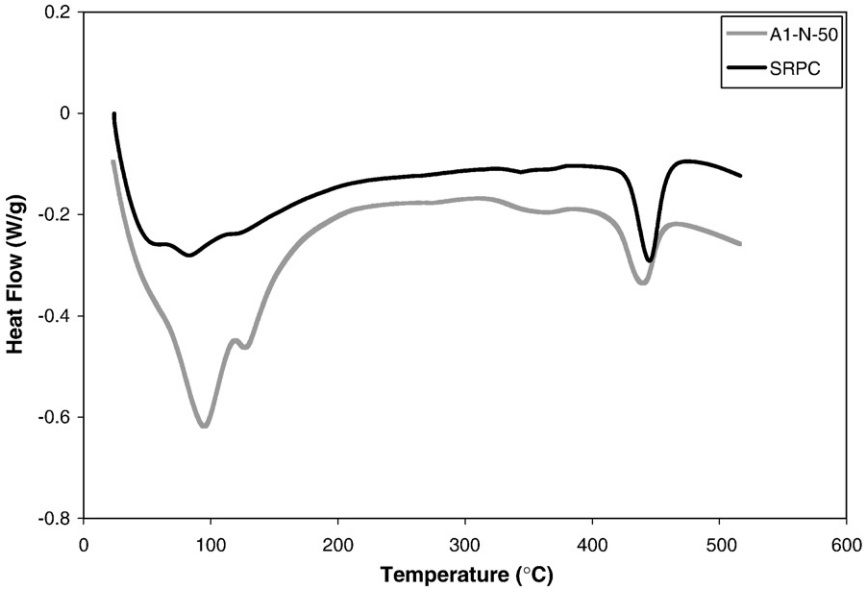

Fig. 11. DSC curves for 100% OPC and 100% SRPC binders after the combined exposure (stress level=0).

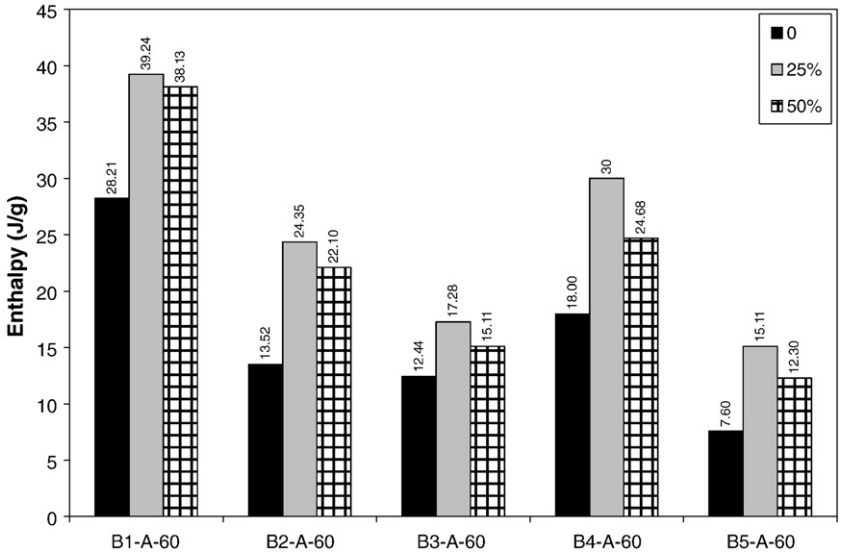

Fig. 12. DSC results for sulfate reaction products (temperature range from 90 to 130 °C) in the surface layer of group B specimens after the combined exposure.

to occur at average temperatures of 90, 110 and 130 °C, respectively [5]. The identification of these phases by DSC alone is sometimes difficult since their dehydroxylation peaks may develop at overlapping temperature ranges (100–130 °C). Therefore, a wide endothermic peak around this range may express intermixed reaction products.

Irrespective of the stress level, physico-mechanical results on specimens subjected to the combined exposure showed that specimens from the SRPC binder performed notably better than similar specimens from the control binder prepared with 100% OPC. Fig. 11 illustrates that cementitious matrices made from SRPC formed smaller quantities of sulfate reaction products relative to similar OPC matrices. A semi-quantitative analysis (by integration of endothermic peaks) of the heat flow curves in Fig. 11 reveals that the amount of ettringite, at a temperature around 92 °C, formed in the OPC paste (32 J/g) was about 8 times higher than that of the SRPC. This observation complies with previous research and field performance [1,4] which confirms the high resistance of SRPC, relative to OPC, to alkali sulfates due to the compositional difference (C_3A content of 1% in the SRPC compared to 9% in the used OPC).

As stated earlier, the blended binders in this study were designed to reduce the portlandite content and dilute the OPC, thus reducing the amount of sulfate-reaction products. This is depicted by Fig. 12, which shows a semi-quantitative analysis of the heat flow curves for some of group B mixtures made from the tested binders after the combined exposure. For example, under a stress level of 25%, the magnitude of formed sulfate reaction products, expressed by the summation of enthalpies of gypsum, ettringite and thaumasite, in the B (B2-A-60), T (B3-A-60), and Q (B4-A-60 and B5-A-60) cementitious matrices were 62, 44 and an average of 57%, respectively of that of the control matrix (B1-A-60). Yet, some specimens from blended binders with reduced portlandite contents had inferior performance under the combined exposure (e.g. A4-N-50, A5-N-50). Thus, unlike in the reference full-immersion exposure, it seems that the approach of limiting the sulfate-bearing products by incorporating various proportions of SCMs in the cementitious binders is not totally effective in mitigating sulfate attack when combined with other damage mechanisms. Apparently, the interplay of different factors governed the degradation of SCC specimens under the combined exposure as will be explained in the succeeding sections of this text.

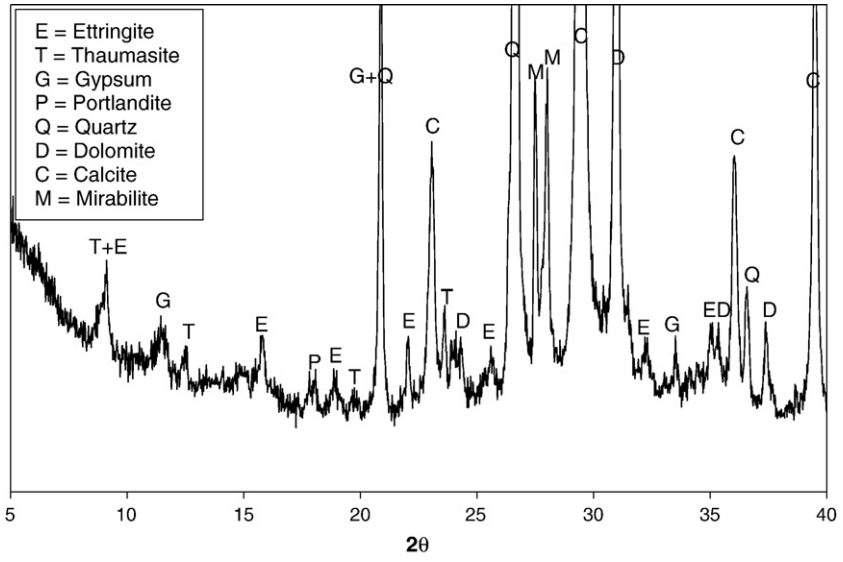

Fig. 13. XRD of powder samples from B4-N-50 specimens (stress level=0) after the combined exposure.

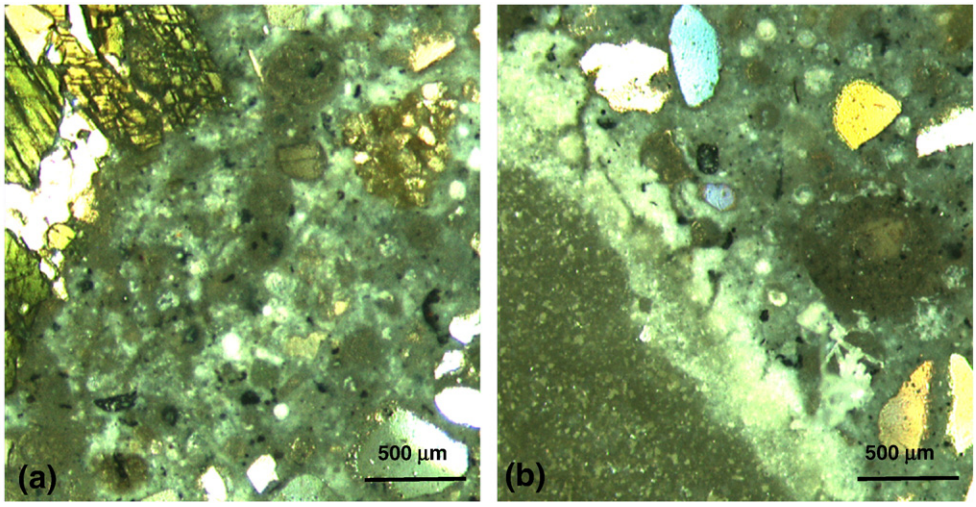

Fig. 14. Thin sections for B4-A-40 specimens (stress level=25%) under polarized light (50X) showing: (a) the mottled appearance of the matrix with thaumasite-filled voids, and (b) aggregate lining with thaumasite.

According to the European [12] and American [13] guidelines for SCC, limestone fillers can have positive effects on the rheological properties of SCC. Hence, relatively high contents of limestone fillers have usually been incorporated in SCC. Some current standards (e.g. BS EN 197-1 [30]) allow up to 35% limestone filler in the total cementitious mass. In the current study, 15% limestone filler was incorporated in a quaternary binder [A4, B4 and C4: 50% OPC, 15% LF, 20% S and 15% FA]. As discussed in the experimental results, under all stress levels, most specimens from this quaternary binder generally had inferior performance (and failed earlier) relative to specimens made with other binders not incorporating limestone filler. As discussed below, DSC, XRD and microscopy analyses revealed the formation of thaumasite in those cementitious matrices incorporating limestone filler.

DSC results (e.g. Fig. 12) show that, under all stress levels, the magnitude of sulfate reaction products in the quaternary binder with 15% LF was consistently higher than that in other blended binders. Heat flow curves for powder samples from this hydrated binder had a wide peak around 102 °C, which reflects an overlapping dehydroxylation range of ettringite and thaumasite. XRD results (e.g. Fig. 13) confirmed the formation of the thaumasite phase in these cementitious matrices along with conventional products of sulfate attack (ettringite and gypsum). Optical microscopy on thin sections from specimens made with the quaternary binder containing limestone filler (B4-A-40) showed an off-white powdery appearance in the cementitious matrix with filled voids and aggregate linings (Fig. 14a–b), which usually indicates the occurrence of an initial stage of thaumasite sulfate attack (TSA).

SEM with EDX analyses confirmed the abundance of thaumasite in the cementitious matrices incorporating limestone filler. Thaumasite was frequently intermixed with other sulfate-bearing phases. For instance, Figs. 15a–b and 16 show the growth of tabular gypsum on extremely fine agglomerates of thaumasite, and the crystallization of intimate ettringite–thaumasite mixtures in a void, respectively. These observations are consistent with previous studies (e.g. [31]) that reported the existence of solid solutions between ettringite and thaumasite. In the above micrographs, the existence of aluminum and silica, respectively, in the EDX spectra of thaumasite and ettringite suggests the formation of thaumasite via the Woodfordite route. According to Bensted [32], in this route, ettringite readily reacts with available C–S–H and carbonate to form thaumasite.

The formation of thaumasite with ettringite and gypsum softened the quaternary cementitious binders incorporating limestone filler and made them more vulnerable to combined exposure damage than hydrated matrices from other blended binders not incorporating limestone filler. While limited thaumasite formation may not necessarily cause damage of cement-based materials, evidence from this study suggests that quaternary mixtures incorporating 15% ultrafine limestone powder suffered an incipient stage of TSA that contributed to early failure and inferior physico-mechanical properties. In the present study,

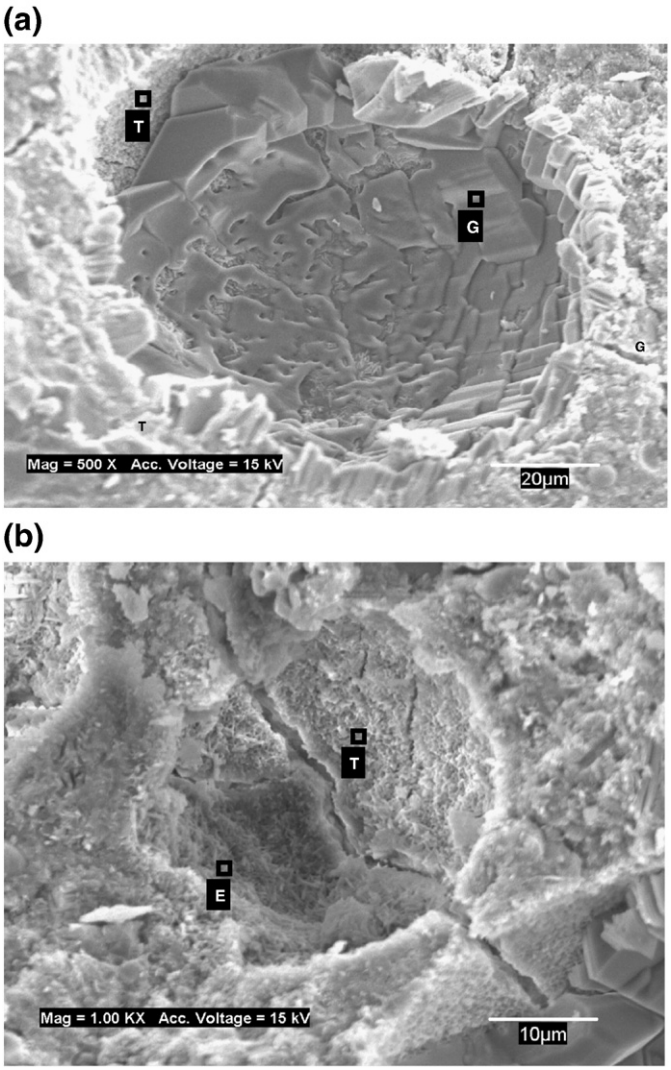

Fig. 15. Typical SEM micrographs for C4-A-H specimens (stress level=25%) showing: (a) the growth of gypsum on thaumasite, and (b) mixed ettringite–thaumasite.

thaumasite, which favourably forms under wet and cold temperatures of less than 15 °C, was also detected in specimens that failed during hot (40 °C) intervals of the combined exposure. It is likely that thaumasite formation mostly occurred during the cold intervals of the exposure and remained stable during the hot intervals. This is consistent with the stability of this mineral up 110 °C [32].

As shown by DSC and XRD analyses, classical products of sulfate attack were formed in other hydrated blended binders without limestone filler, which had lower enthalpies in Fig. 12. For instance Fig. 17, shows the formation of ettringite and gypsum in a diffractogram of specimens from the ternary binder (B3-A-60). Incidental features of thaumasite formation were observed under SEM and XRD in those binders without limestone filler. Nobst and Stark [33] suggested that this may be ascribed to the high Al_2O_3 content in SCMs, which may act as precursor for ettringite and consequently thaumasite formation through the Woodfordite route. Perhaps, the source of carbonates in such matrices was derived from the proportion of dolomite/dolomitic aggregates in the used crushed stone.

6.2. Effect of air-entrainment

Results of the combined exposure show that air-entrainment in specimens from group B mixtures led to better performance than that of the corresponding specimens from group A mixtures. While some specimens (e.g. SRPC specimens) from group A survived the combined exposure up to 360 days, others showed early failure (e.g. 27 days), particularly under the high stress level of 50%. Comparatively, at the stress level of 50%, the earliest failure among the air-entrained SCC specimens from group B occurred after 97 days of exposure (Fig. 6). At early stages of the combined tests, DSC and XRD analyses showed no appreciable formation of sulfate reaction products in non-air-entrained matrices, especially in those from blended binders owing to their low portlandite content and OPC dilution as explained earlier. This implies that early failure of specimens from the control and blended binders from group A mixtures occurred primarily due to a lack of air-entrainment considering the exposure to freezing–thawing cycles. While the performance of non-air-entrained SCC specimens depended on specific materials combinations and testing conditions, all the air-entrained specimens consistently showed better durability under the combined exposure. Such results are consistent with earlier work by the authors [34], which outlined the risk of non-air-entrained high-performance concrete under field conditions in cold climates.

Under combined exposure, multiple deleterious mechanisms occurred within the cementitious matrix, including tensile stresses from cyclic environmental conditions (alternating freezing–thawing and wetting–drying cycles) and formation of voluminous sulfate-bearing phases. Apparently, the existence of a network of well dispersed air-bubbles in the SCC matrix effectively acted as a buffer for relieving hydraulic and osmotic pressures and a host for the nucleation and crystallization of sulfate-bearing products. Indeed, this decreased the expansion of SCC specimens from group B (Table 4), and thus reduced the damage. This was supported by optical microscopy and SEM

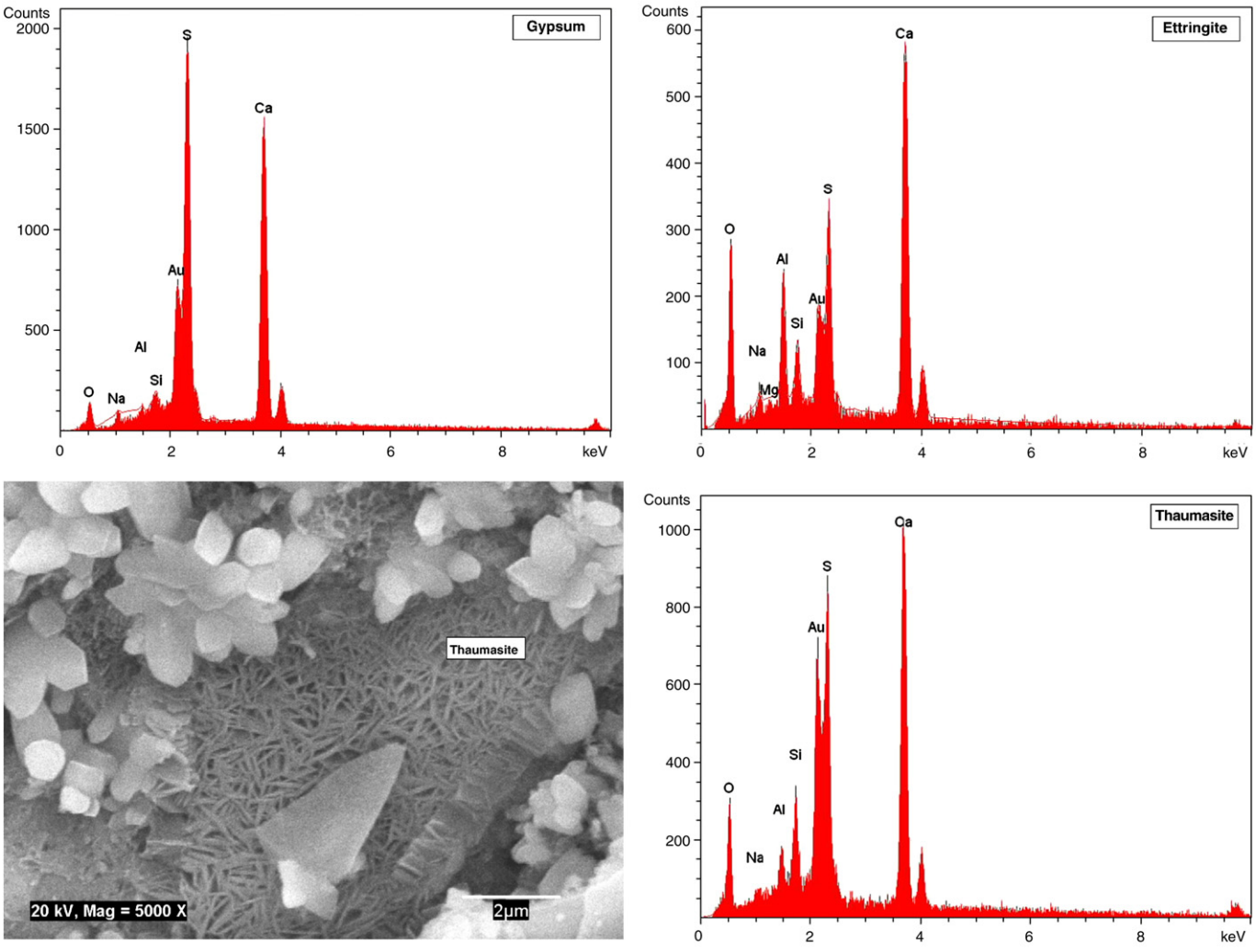

Fig. 16. EDX spectra and a close-up of the very fine structure of thaumasite for the areas marked in Fig. 15.

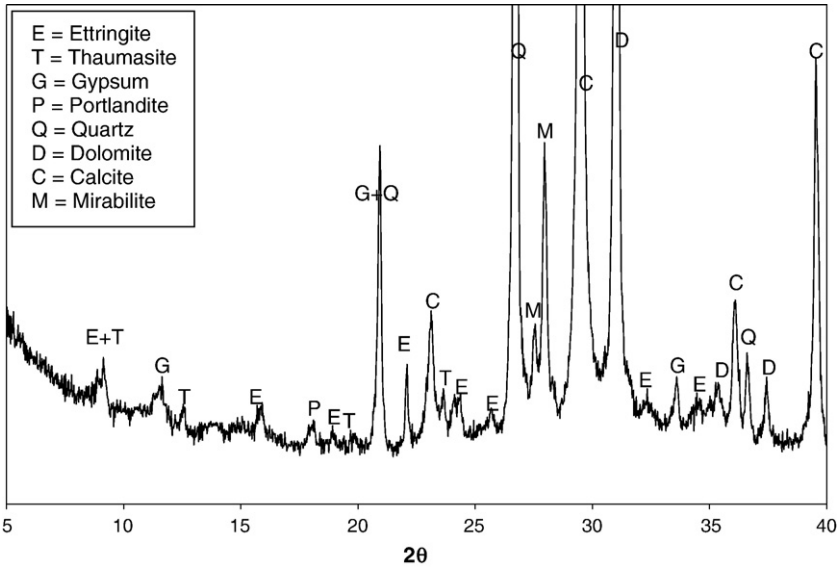

Fig. 17. XRD of powder samples from B3-A-60 specimens (stress level=25%) after the combined exposure.

analyses (e.g. Fig. 18a–b) that show partial to complete infilling of voids depending upon the degree of deterioration. The extent of damage depended on the combined effects of the multiple damage mechanisms involved in the combined exposure as will be explained below. It is worth noting that continual infilling of air-entrained cementitious matrices will eventually impair their resistance to frost action and may contribute to an abrupt failure by transverse macro-cracks.

6.3. Effect of sand-to-aggregate ratio

Statistical analysis by ANOVA showed that the effect of varying the S/A from 40 to 60% in group B mixtures did not have a significant effect on results under the combined exposure. The physico-mechanical results depended mainly on the characteristics of the bulk cementitious paste (the type of binder and air-entrainment) as explained earlier. Under the cyclic environments (freezing–thawing and wetting–drying) micro-cracking invariably spread in the bulk cementitious paste and affected the overall performance of specimens. Indeed, micro-cracking of the bulk cementitious paste was intensified in the case of sustained loading, as will be explained later in the text.

6.4. Effect of fibres

The incorporation of hybrid fibres in SCC at a low volume of 0.5% aimed at combining the advantageous effects of polymer micro-fibres and steel macro-fibres. According to Johnston [35], polymer micro-fibres may positively contribute to the pre-crack behaviour by impeding the nucleation and coalescence of micro-cracks, while steel macro-fibres can

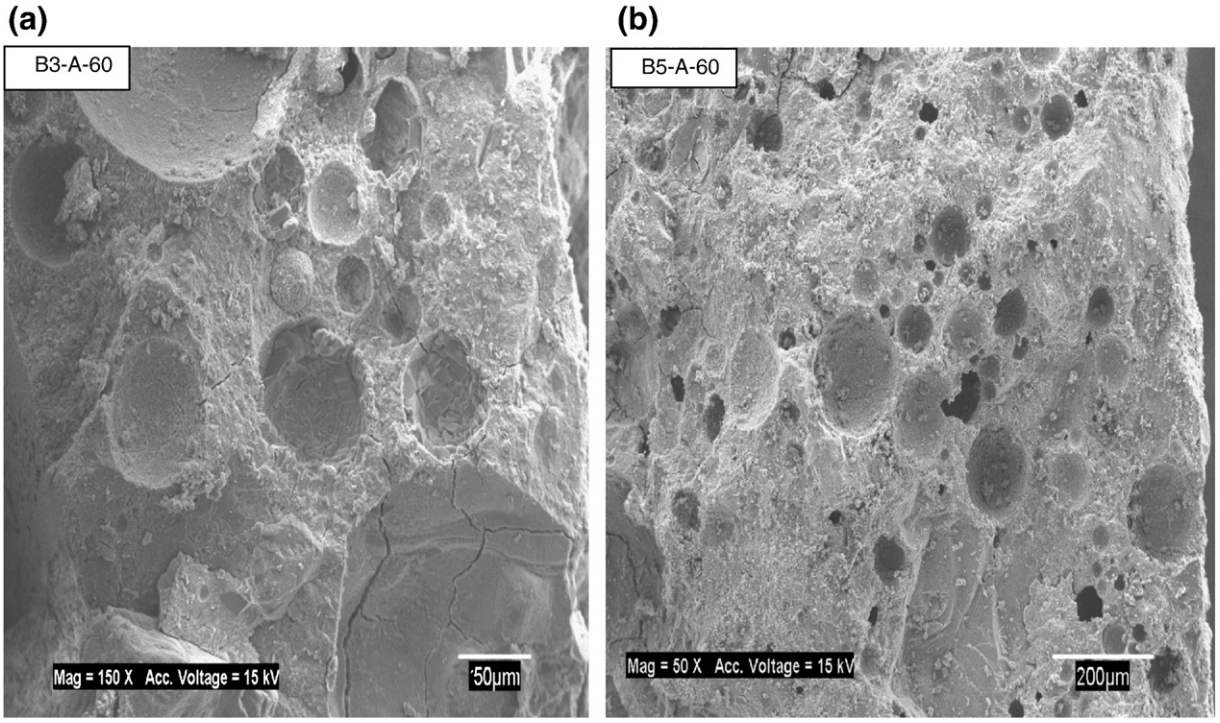

Fig. 18. SEM micrographs showing voids infilling in initially air-entrained matrices after the combined exposure from: (a) B3-A-60, and (b) B5-A-60 specimens.

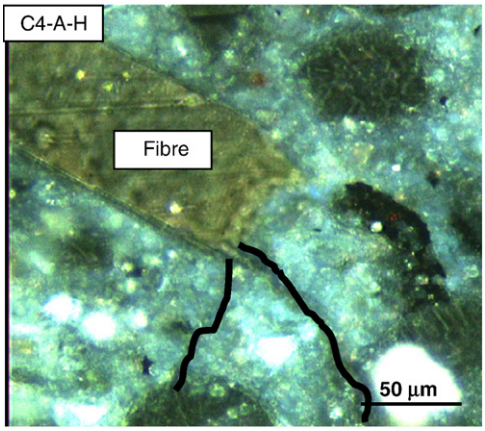

Fig. 19. A thin section from a C4-A-H specimen (stress level = 50%) under polarized light (500X) showing crack arresting by micro-fibres.

bridge macro-cracks, thus contributing to the control of crack propagation. In this study, the effect of hybrid fibres was evident in controlling the expansion of SCC specimens, regardless of the binder type, compared to results of non fibre-reinforced specimens from group A and B mixtures. Optical microscopy further highlighted the role of fibres in controlling the internal cracking of specimens, particularly at the inner core of the cementitious matrix. For instance, Fig. 19 shows a typical crack arresting behaviour by micro-fibres at 30 mm depth from the exposed surface.

Conversely, under the combined exposure, most SCC specimens with hybrid fibre reinforcement exhibited a significant reduction in the first cracking stress/and or started to break earlier compared to corresponding non fibre-reinforced specimens from group B. This was mainly attributed to the corrosion of surface steel fibres under the severe cyclic environmental conditions of intermittent wetting (sodium sulfate) and drying (hot seasons) cycles. Fig. 20a illustrates the corrosion of surface steel fibres and associated spalling of the concrete surface. The surface deterioration of steel fibres was worse under sustained flexural stress due to the increased cracking and vulnerability of steel to the phenomenon of stress-corrosion (combination of chemical media with flexural stress). Under sustained flexural stress loading, concrete specimens were exposed to maximum tensile stresses at the bottom surface (maximum distance from the neutral axis) of the middle-third span of prismatic specimens. The existence of deteriorated/corroded surface steel fibres in locations subjected to the highest tensile stresses created the weakest link and invoked first cracking at relatively low stress levels. Visual inspection showed that there was no corrosion of steel fibres in the bulk cross-section (Fig. 20b).

Fig. 20c shows a relatively wide crack opening with some spalling of concrete in a specimen from the binary binder (C2-A-H) under a stress level of 50%. Fracture of corroded steel fibres at the bottom surface initiated the first crack after 173 days of exposure, which opened a direct path for the sodium sulfate solution to the inner specimen core. With progressive widening of the crack due to the sustained flexural load, corroded steel fibres at the surface failed to bridge the crack and broke.

Some researchers [e.g. [36]] stated that the effect of corrosion of surface steel fibres is not detrimental to fibre-reinforced cement composites in field conditions. However, in the present study, the creation of weak zones at the surface of specimens due to corrosion of steel fibres caused surface cracking at low stress levels and opened direct paths to the ingress of aggressive media. This warrants caution in applications using steel fibre-reinforced cement composites in

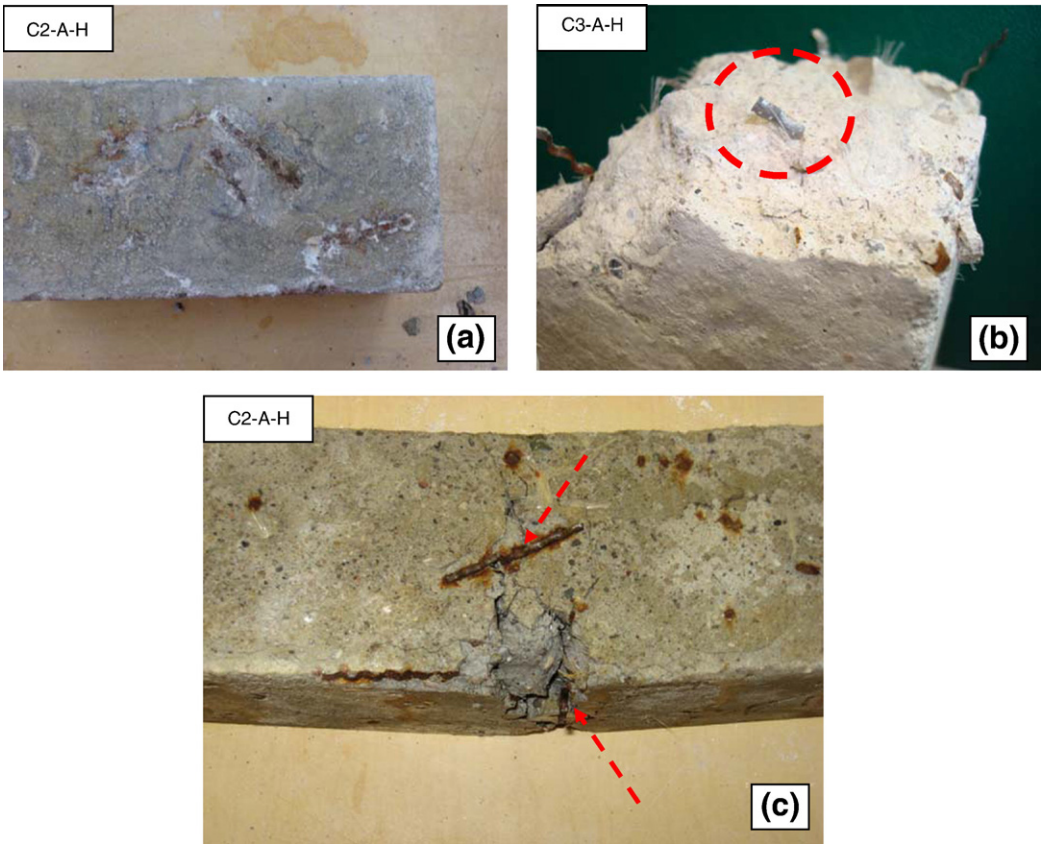

Fig. 20. (a) Corrosion of surface steel fibres and associated spalling, (b) non-corroded steel fibre in the bulk core, and (c) crack initiation and widening through breakage of corroded fibres (stress level = 50%).

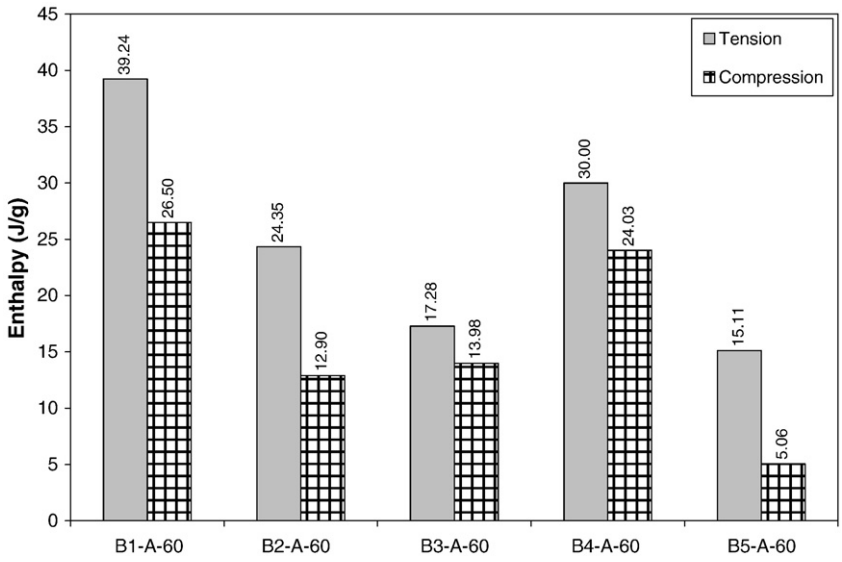

Fig. 21. Enthalpies of sulfate reaction products (temperature range from 90 to 130 °C) in the tension and compression surfaces of group B specimens after the combined exposure (stress level=25%).

aggressive chemical environments, especially under sustained combined flexural loading and wetting–drying conditions.

6.5. Effects of multiple damage mechanisms

From the above discussion it can be deduced that coupling cyclic environmental conditions and flexural stress with sodium sulfate exposure enhanced the damage mechanisms and rate of attack due to additive and combined effects. The combination of sodium sulfate with flexural stress caused stress–corrosion (acceleration of crack-propagation due a sustained flexural stress in a corrosive chemical environment) of the cementitious matrix that led to sudden failure of several specimens, particularly under the high stress level of 50% (Fig. 6). On the other hand, the generation of micro-cracks due to the sustained flexural stress in the tension zone of specimens increased the penetrability of the sodium sulfate solution into SCC specimens and accelerated the kinetics of sulfate attack compared to that for the reference full-immersion exposure. This is depicted in Fig. 21 which shows that the magnitude of sulfate-bearing phases formed in the surface layer (0–15 mm depth) of the tension zone was 1.24 to 3 times higher than that formed in the compression zone for the same specimens. Moreover, EDX elemental spatial distribution maps on thin sections (e.g. Fig. 22a–b) showed the abundance of sodium (Na) and sulfur (S) through a considerable depth of the section of a 25% flexural stress loaded (B2-A-60) specimen in contrast to a limited zone at the surface in the corresponding non-loaded specimen.

The effect of increasing the flexural stress level on aggravating sulfate attack is shown in Fig. 12. It can be observed that the magnitude of sulfate-bearing phases in the tension zones of loaded (25 and 50% stress levels) specimens was consistently higher than that of non-loaded specimens. To

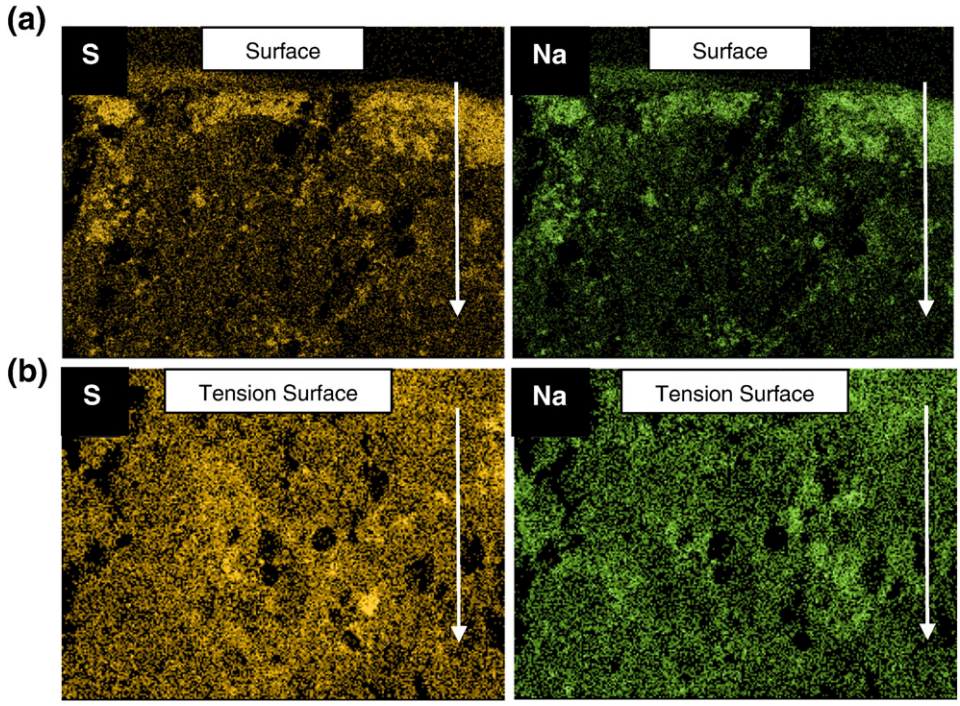

Fig. 22. Elemental spatial distribution in thin sections from: (a) non-loaded, and (b) loaded (stress level=25%) B2-A-60 specimens after the combined exposure.

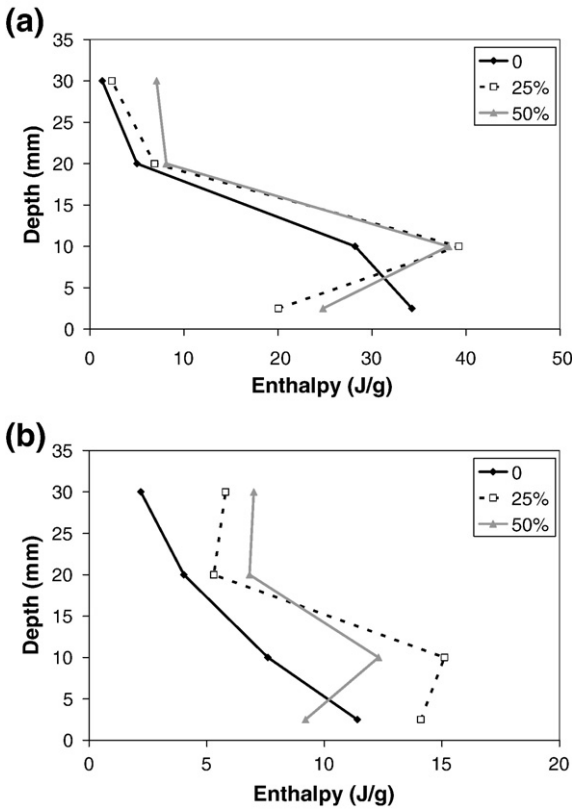

Fig. 23. Enthalpies of sulfate reaction products (temperature range from 90 to 130 °C) vs. depth for: (a) B1-A-60, and (b) B5-A-60 specimens.

capture the effect of the increase in the stress level from 25 to 50% on the extent of damage, DSC analyses were conducted on powder samples from selected specimens at variable depths (0–5, 5–15, 15–25 and 25–35 mm) from the exposed tension face. Figs. 23a–b show shows the magnitude of sulfate-bearing products versus the depth at which they formed for the control specimens (B1-A-60) and specimens from the quaternary binder without limestone filler (B5-A-60) at the end of exposure. It can be observed that the increase of the stress level from 0 to 50% increased the penetrability of sodium sulfate into deeper regions of the specimens as implied by an increase of the formed sulfate-bearing phases. Hence, when specimens were subjected to flexural stress, sodium sulfate found direct paths to penetrate further into the cementitious matrix, which accelerated the kinetics of sulfate reactions and failure of specimens due to stress–corrosion. Obviously, relating the kinetics of damage to pure sulfate diffusion into the cementitious matrix is erroneous in this case.

The combination of freezing–thawing and wetting–drying cycles with exposure to a sodium sulfate solution also accelerated the rate of damage compared to that of the reference full-immersion exposure. Alternating freezing–thawing and wetting–drying cycles induced micro-cracks (e.g. Fig. 24) in the cementitious matrix, even without sustained flexural load. The increased penetrability of the solution accelerated the damage rate as indicated by the aggravated deterioration of physico–mechanical properties. The situation was even more complicated when a sustained flexural load was also applied, leading in several cases to breakage of specimens (Figs. 5c–d and 6). This combined effect of stress–corrosion under cyclic environments was especially notable for non-air-entrained SCC specimens from group A (A4-N-50 and A5-N-50), which started to fail at early stages of the test.

The effect of coupling cold temperature with the sodium sulfate solution was evident in the development of TSA in specimens made with quaternary binders incorporating 15% limestone filler. Moreover, due to the continual supply of the sodium sulfate solution, both actions of freezing–thawing and wetting–drying under hot temperature promoted the crystallization of sodium sulfate in the surface layer of specimens due to supersaturation. XRD (e.g. Figs. 13 and 17) showed the existence of crystalline mirabilite ($Na_2SO_4{\cdot}10H_2O$) in most powder samples collected from a depth in the range of 0–15 mm from the exposed surfaces. SEM and EDX on fracture surfaces confirmed the crystallization of sodium sulfate nearing the surface (Fig. 22a) and in voids and fissures (Figs. 22b and 25a). Progressive built-up of salt under cycling temperatures can also lead to differential salt concentrations within the surface layer of specimens and associated osmotic pressures. The combined effect of salt crystallization and osmotic pressures principally led to the observed surface scaling during freezing–thawing and wetting–drying cycles.

It has been reported that wetting (even with pure water)–drying cycles of concrete, may lead to recrystallization of ettringite, which is classified under the phenomenon of delayed ettringite formation (DEF) [37]. In this study, secondary ettringite and gypsum formed by the reactions of sodium sulfate with the cementitious paste (Eqs. (1) and (2)). Yet, varying the moisture conditions during the simulated hot seasons might have contributed to recrystallization of secondary ettringite into large crystals. Fig. 25b shows an SEM micrograph of a void completely filled by ettringite crystals of variable size and thickness. This is attributed to the phenomenon known as Ostwald Ripening, which refers to the growth of large crystals at the expense of smaller ones to attain reduction in energy (less surface-to-volume ratio) [38].

With the progress of damage under the combined exposure, optical microscopy on polished thin sections (e.g. Fig. 26) showed the formation of low density surface zones (about 10 mm thick) relative to the inner core. Microanalysis showed that these zones had abundant micro-cracks and depositions of voluminous sulfate reaction products and salt crystals that preferentially nucleated and grew in voids forming intimate assemblages (Figs. 15, 16, 18, 22, 25a–27). Salt crystallization together with sulfate reaction products in the confined pore space can exert large stresses leading to further cracking. The occurrence of this complex form of salt crystallization with sulfate attack reaction phases was also shown by XRD (Figs. 13 and 17). Accumulation of sulfate attack reaction products and salt crystallization near the exposed surfaces created an expanding zone relative to the restraining (non-expanding/unaltered) core. This likely induced tensile stresses which combined with flexural loading is believed to have initiated the breakage of loaded SCC specimens.

7. Conclusions

With the growing use of SCC in various infrastructure applications exposed to combined sulfate attack, cyclic environmental conditions and flexural loading, it has become necessary to investigate the

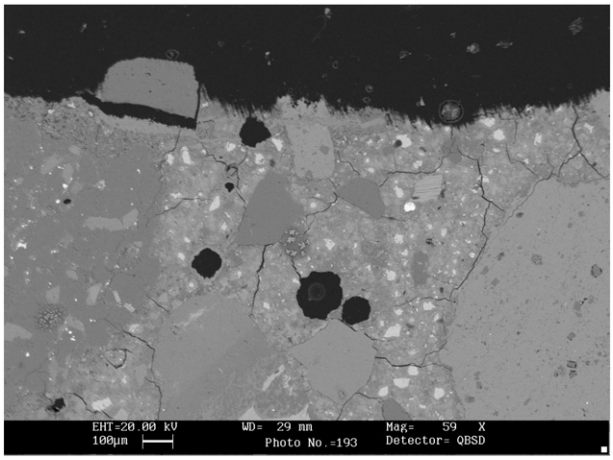

Fig. 24. BSEM micrograph showing micro-cracking of a non-loaded A1-N-50 specimen due to cyclic environments.

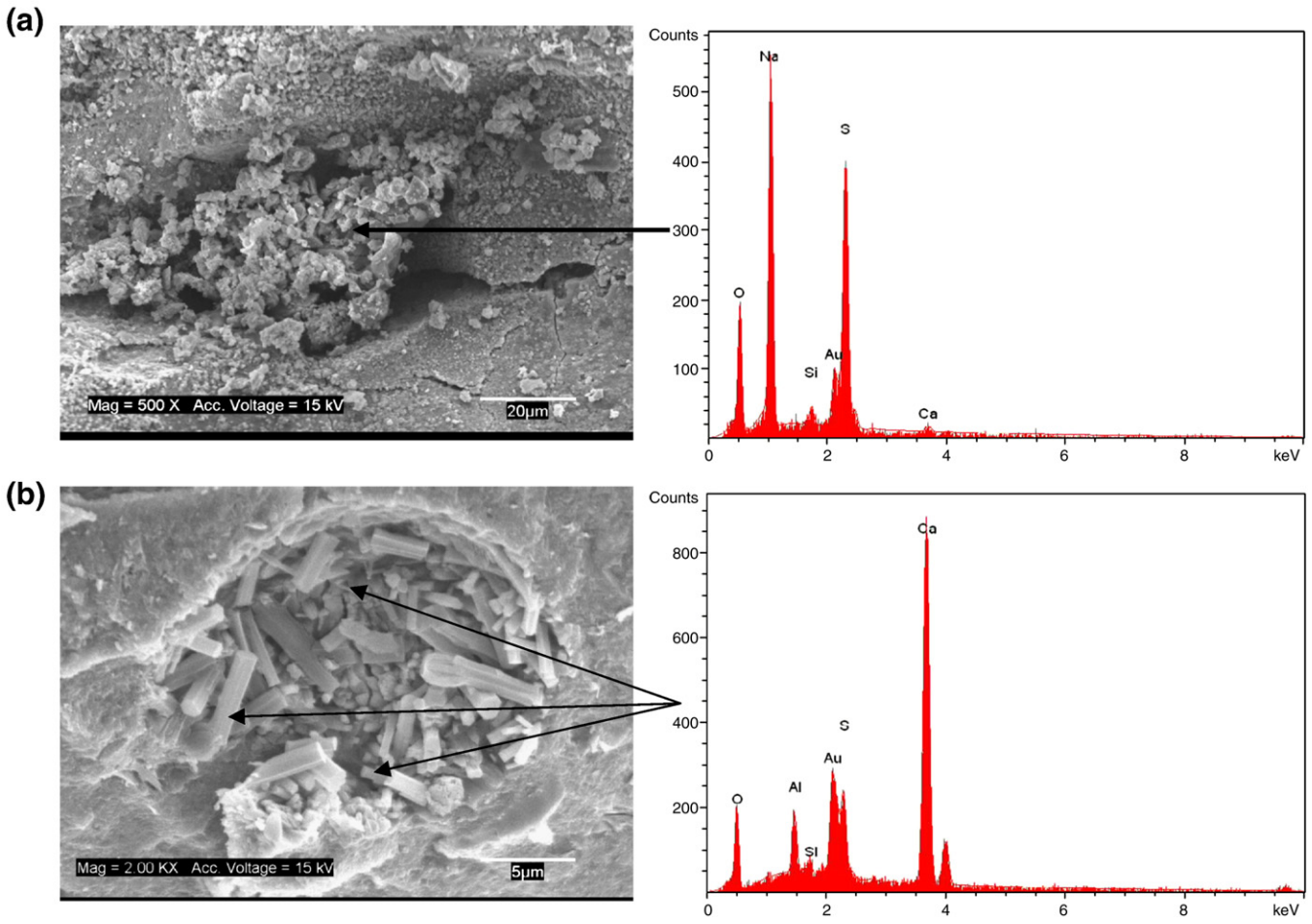

Fig. 25. SEM micrographs for fracture surfaces from: (a) B2-A-60, and (b) B3-A-60 specimens, showing salt crystallization in fissures and recrystallization of ettringite (Ostwald Ripening), respectively.

suitability of a wide range of SCC mixture designs to such environments. Considering the mixture designs, concentration and type of sulfate solution used and the combined testing approach implemented in the present study, the following conclusions can be drawn:

- Based on the performance in the full-immersion exposure, all the tested SCC mixtures can qualify for use in 'very severe' alkali sulfate exposure. Unlike in the holistic testing approach implemented in this study, the reference exposure could not capture potential risks that may arise if cyclic environmental conditions and flexural loading are combined with sodium sulfate exposure.
- In the case of combined exposure, cyclic environmental conditions and flexural loading caused cracking in the cementitious matrix and led to direct ingress of the solution into considerable depths of the

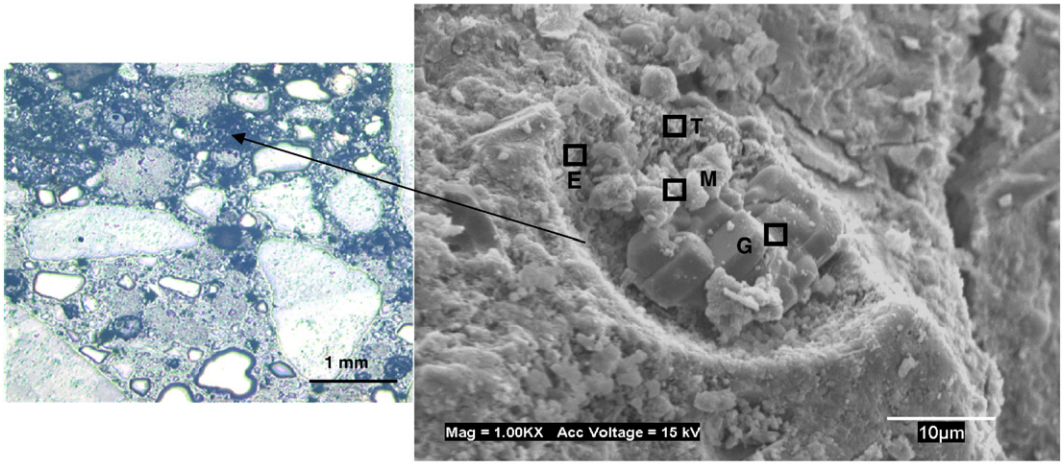

Fig. 26. A deteriorated zone in a B3-A-60 specimen (stress level=25%) under plain light (25X), and a typical SEM micrograph from this zone showing accumulation of salt crystallites (M=mirabilite) with sulfate reaction products (E=ettringite, G=gypsum, T=thaumasite) in a void.

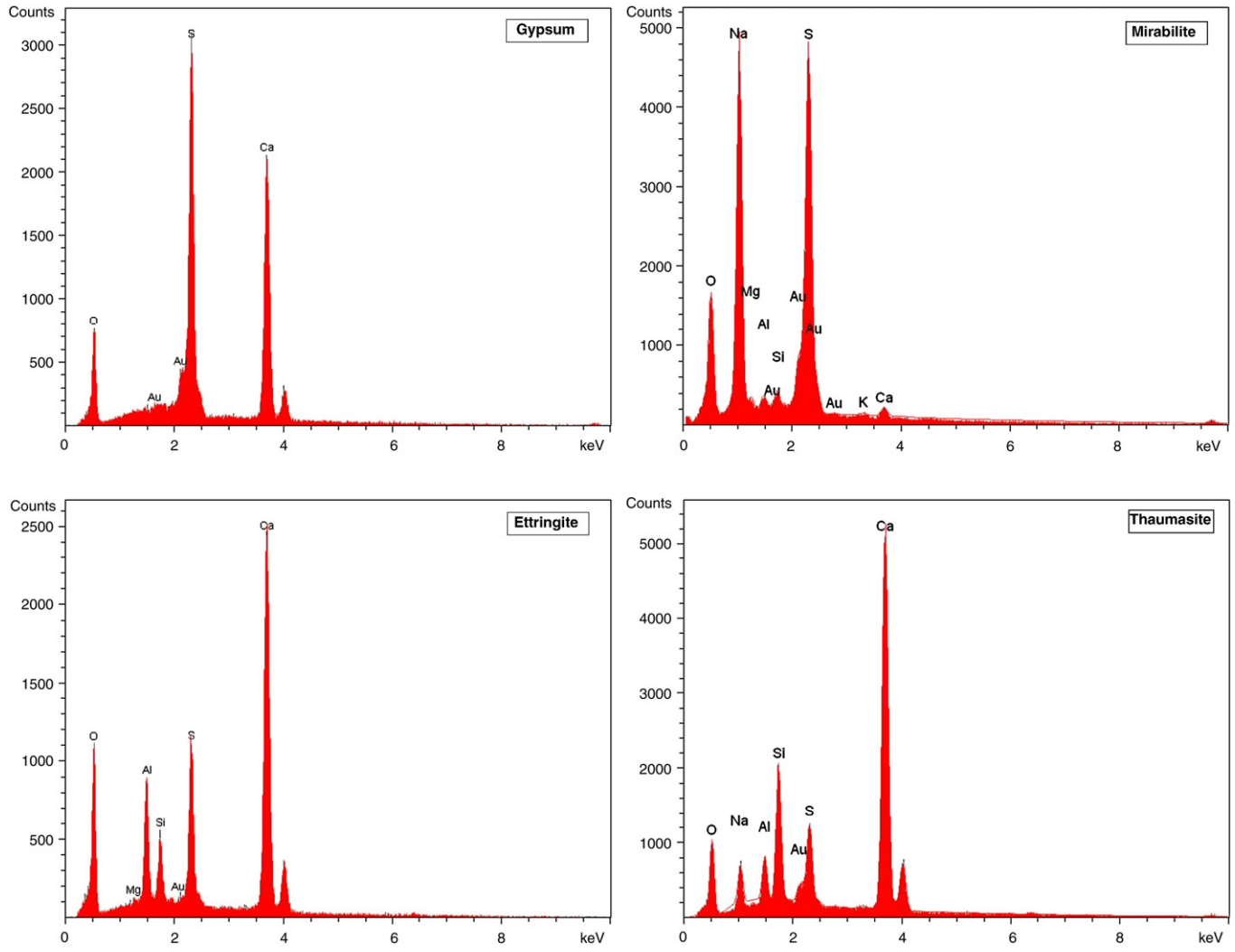

Fig. 27. EDX spectra for the marked points in Fig. 26.

SCC specimens. Obviously, replicating the ingress of sulfate ions through pure diffusion alone is invalid in such a case.

- The conventional approach of incorporating proportions of SCMs in the cementitious matrix to mitigate sulfate attack may not be fully effective under real in-service exposure since other factors than the binder type seemed to affect the damage process under a combined field-like exposure.
- The quaternary binder incorporating limestone filler (commonly used in SCC mixtures) exhibited consistently inferior performance, mainly due to the combined effect of sodium sulfate and cold temperatures that led to incipient thaumasite sulfate attack (TSA). Such a performance risk should be accounted for when qualifying SCC mixtures for use in environments conductive to TSA.
- The practice of air-entrainment is indispensable in cold climates to safely extend the service life of concrete elements exposed to successive freezing–thawing cycles. Entrained air bubbles offered host locations for the nucleation and growth of sulfate reaction products and salt crystallization, thus reducing the rate of damage.
- Variation in the sand-to-aggregate ratio had statistically insignificant effect on the physico-mechanical properties of SCC specimens subjected to the combined exposure.
- While the incorporation of hybrid fibre reinforcement controlled the expansion of SCC specimens, the existence of corroded steel fibres on the surface provoked the first-cracking at relatively low stress levels, which can cause serviceability problems under similar combined exposure.
- The accumulation of voluminous sulfate reaction products with salt crystallization created expanding zones at exposed surfaces, which when coupled with flexural loading seemed to increase the net tensile stresses, and thus initiated the breakage of specimens.
- Overall, the field-like combined exposure to cyclic environments, flexural loading and sodium sulfate solution had additive and perhaps synergistic effects on SCC specimens, causing the coexistence of multiple-complex degradation mechanisms (sulfate attack, TSA, stress–corrosion, salt crystallization, surface scaling and corrosion of surface steel fibres) depending on the mixtures design variables. This is fundamentally different from studying a single damage mechanism (sulfate attack) acting on SCC in simple immersion tests.
- The findings of this study reveal that in addition to the current standards and specifications for concrete, much research should be conducted to develop performance standards and specifications that consider the combined actions of chemical, physical and structural mechanisms. This should lead to producing more reliable data on the durability of normal and emerging concretes with expected improvements in the durability-based design methods and life-cycle modelling of concrete structures.

Acknowledgements

The continued support of the Natural Science and Engineering Research Council of Canada (NSERC) to M. L. Nehdi is highly

appreciated. Funding of the Ontario Innovation Trust (OIT) and the Canada Foundation for Innovation (CFI) that allowed creating a state-of-the-art laboratory in which these experiments were conducted has been crucial to this research. M. T. Bassuoni acknowledges the Ontario Graduate Scholarship (OGS) for partially supporting his doctoral studies.

References

[1] J. Skalny, J. Marchand, I. Odler, Sulfate Attack on Concrete, Spon Press, UK, 2002.
[2] P.K. Mehta, Sulfate attack on concrete: separating myths from reality, Concr. Int. 22 (8) (2000) 57–61.
[3] A. Neville, The confused world of sulfate attack on concrete, Cem. Concr. Res. 34 (8) (2004) 1275–1296.
[4] P.C. Hewlett, Lea's Chemistry of Cement and Concrete, Arnold, UK, 1998.
[5] M. Santhanam, Studies on Sulfate Attack: Mechanisms, Test Methods, and Modeling, PhD Thesis, Purdue University, U.S., 2001.
[6] P. Brown, H. Taylor, The role of ettringite in external sulfate attack, in: J. Marchand, J. Skalny (Eds.), Materials Science of Concrete Special Volume: Sulfate Attack Mechanisms, The American Ceramic Society, 1999, pp. 73–98.
[7] N. Crammond, The thaumasite form of sulfate attack in the UK, Cem. Concr. Compos. 25 (8) (2003) 809–818.
[8] P. Hagelia, R. Sibbick, N. Crammond, C. Larsen, Thaumasite and secondary calcite in some Norwegian concretes, Cem. Concr. Compos. 25 (8) (2003) 1131–1140.
[9] S. Sahu, S. Badger, N. Thaulow, Evidence of thaumasite in Southern California concrete, Cem. Concr. Compos. 24 (3–4) (2003) 379–384.
[10] J. Skalny, J. Pierce, Sulfate attack: an overview, in: J. Marchand, J. Skalny (Eds.), Materials Science of Concrete Special Volume: Sulfate Attack Mechanisms, The American Ceramic Society, 1999, pp. 49–63.
[11] J. Clifton, G. Frohnsdorff, C. Ferraris, Standards for evaluating the susceptibility of cement-based materials to external sulfate attack, in: J. Marchand, J. Skalny (Eds.), Materials Science of Concrete Special Volume: Sulfate Attack Mechanisms, The American Ceramic Society, 1999, pp. 337–355.
[12] The European Guidelines for Self-Compacting Concrete, BIBM, CEMBUREAU, ERMCO, EFCA, EFNARC, www. efnarc.org, 2005, 63 p.
[13] ACI 237R-07, Self-Consolidating Concrete, American Concrete Institute, Farmington Hills, MI, USA, 2007, 30 pp.
[14] W. Zhu, J. Bartos, Permeation properties of self-compacting concrete, Cem. Concr. Res. 33 (6) (2003) 921–926.
[15] V. Boel, K. Audenaert, G. De Schutter, G. Heirman, L. Vandewalle, B. Desmet, J. Vantomme, Transport properties of self compacting concrete with limestone filler and fly ash, Mat. Struct. 40 (5) (2007) 507–516.
[16] B. Persson, Sulphate resistance of self-compacting concrete, Cem. Concr. Res. 33 (12) (2003) 1933–1938.
[17] M. Nehdi, M. Pardhan, S. Koshowski, Durability of self-consolidating concrete incorporating high-volume replacement composite cements, Cem. Concr. Res. 34 (11) (2004) 2103–2112.
[18] C. Miao, R. Mu, Q. Tian, W. Sun, Effect of sulfate solution on the frost resistance of concrete with and without steel fiber reinforcement, Cem. Concr. Res. 32 (1) (2002) 31–34.
[19] U. Schneider, E. Nägele, F. Dumat, Stress corrosion initiated cracking of concrete, Cem. Concr. Res. 16 (4) (1986) 535–544.
[20] U. Schneider, W. Piasta, The behaviour of concrete under Na_2SO_4 solution attack and sustained compression or bending, Mag. Concr. Res. 43 (157) (1991) 281–289.
[21] U. Schneider, S. Chen, Behavior of high-performance concrete under ammonium nitrate solution and sustained loading, ACI Mater. J. 96 (1) (1999) 47–51.
[22] ASTM C 1012, Standard Test Method for Length Change of Hydraulic-cement Mortar Exposed to a Sulfate Solution, American Society for Testing and Materials, Philadelphia, PA, 2002.
[23] M. Nokken, R.D. Hooton, C. Rogers, Measured internal temperatures in concrete exposed to outdoor cyclic freezing, Cem. Concr. Aggr. 26 (1) (2004) 26–32.
[24] ASTM C 215, Standard Test Method for Fundamental Transverse, Longitudinal, and Torsional Resonant Frequencies of Concrete Specimens, American Society for Testing and Materials, Philadelphia, PA, 2002.
[25] ASTM C 78, Standard Test Method for Flexural Strength of Concrete Using Simple Beam with Third-Point Loading, American Society for Testing and Materials, Philadelphia, PA, 2002.
[26] ACI 201.2R-01, Guide to Durable Concrete, American Concrete Institute, Farmington Hills, MI, USA, 2001, 40 pp.
[27] P. Brown, An evaluation of the sulfate resistance of cements in a controlled environment, Cem. Concr. Res. 11 (5–6) (1981) 719–727.
[28] M. Cohen, B. Mather, Sulfate attack on concrete-research needs, ACI Mater. J. 88 (1) (1991) 62–69.
[29] D. Montgomery, Design and Analysis of Experiments, John Wiley & Sons, New York, 2001.
[30] BS EN 197-1, Cement – Composition, Specifications and Conformity Criteria for Common Cements, British Standards Institution, London, 2000.
[31] S. Barnett, C. Adam, A. Jackson, Solid solutions between ettringite, $Ca_6Al_2(SO_4)_3(OH)_{12}{\cdot}26H_2O$, and thaumasite, $Ca_3SiSO_4CO_3(OH)_6{\cdot}12H_2O$, J. Mater. Sci. 35 (16) (2000) 4109–4114.
[32] J. Bensted, Thaumasite-direct, woodfordite and other possible formation routes, Cem. Concr. Compos. 25 (8) (2003) 873–877.
[33] P. Nobst, J. Stark, Investigations on the influence of cement type on thaumasite formation, Cem. Concr. Compos. 25 (8) (2003) 899–906.
[34] M.T. Bassuoni, M. Nehdi, The case for air-entrainment in high performance concrete, ICE Struct. Build. 158 (5) (2005) 311–319.
[35] C. Johnston, Fiber-Reinforced Cements and Concretes, Gordon and Breach Science Publications, The Netherlands, 2001.
[36] J. Sustersic, A. Zajc, I. Leslovar, R. Ercegovic, Study of corrosion resistance of steel fibres in SFRC, in: B. Oh, K. Sakai, O. Gjorv, N. Banthia (Eds.), Concrete under Severe Conditions: Environment and Loading (CONSEC'04), 2, Seoul National University and Korean Concrete Institute, 2004, pp. 1540–1547.
[37] J. Stark, K. Bollmann, Laboratory and field examinations of ettringite formations in pavement concrete, in: B. Erlin (Ed.), Ettringite: The Sometimes Host of Destruction, ACI SP-177, 1999, pp. 183–198.
[38] R. Boistelle, J. Astier, Crystallization mechanisms in solution, J. Cryst. Growth 90 (1–3) (1988) 14–30.